Design and Analysis of Robots that Perform Dynamic Tasks Using Internal Body Motion

by

Kevin Lawrence Brown

B.S.M.E., Massachusetts Institute of Technology
(1988)

M.S.M.E.,Massachusetts Institute of Technology
(1990)

Submitted to the Department of Mechanical Engineering
in partial fulfillment of the requirements for the degree of

DOCTOR OF PHILOSOPHY

at the

MASSACHUSETTS INSTITUTE OF TECHNOLOGY

September, 1994

Signature of Author _____
Department of Mechanical Engineering
July, 1994

Certified by _____
Haruhiko Asada
Professor of Mechanical Engineering
Thesis Supervisor

Accepted by _____
Ain A. Sonin
Chairman, Graduate Committee

Design and Analysis of Robots that Perform Dynamic Tasks Using Internal Body Motion

by

Kevin Lawrence Brown

Submitted to the department of Mechanical Engineering on June 17, 1994, in partial fulfillment of the requirements for the degree of Doctor of Philosophy

A new approach to robot design and control specifically for dealing with heavy loads is presented in this thesis. Inspired by human dynamic motion, we explore dynamic task strategies to create large forces by dynamically moving the internal body. This technique can produce a much greater force than the traditional quasi-static technique. The strategy of this dynamic task performance is three-fold. One is to store a large momentum in the internal body motion and discharge the momentum at the interaction between the robot's end-effector and the environment. Second, the robot takes advantage of specific postures of the arm and leg to create a large mechanical advantage which allows for efficient load bearing and transmission of actuator torques to the end-effector. Third, peak outputs of robot actuators are utilized for short periods of time. These peak outputs can be up to an order-of-magnitude higher than their continuos rated torques.

The basic concept of this dynamic task strategy is described along with two exemplary case studies: dynamic lifting of a heavy weight and opening a stuck door. Kinematic and dynamic behavior of robots is analyzed, and conditions for the robot structure to perform such dynamic tasks are obtained. The dynamic trajectory of the internal body motion as well as one for the end effector motion are optimized by parametric representation of dynamic task performance. The performance index is based on the heat dissipated in the robot's motors. Initial parameter estimates for the optimization were derived from data measured of human motion. Simulation of the lifting task found that a robot designed with the appropriate motors and gear ratios requires 46% less dissipated energy using the dynamic method compared to a non-coordinated trajectory approach. A prototype robot is designed, built and tested. Experiments demonstrate the feasibility and effectiveness of the dynamic task strategies.

Thesis Supervisor: Haruhiko Asada, Professor of Mechanical Engineering

Acknowledgments

I would like to thank Prof. Asada, for if it were not for his zealous encouragement, his guidance and writing lessons, I would never have written anything like this thesis. I would also like to thank Dr. J. Ken Salisbury and Prof. Woody Flowers for their support and guidance as committee members.

I am grateful for the love, technical support, and understanding from my wonderful girlfriend Susanna Leveroni. If it were not for her help I would have never finished. I would like to tell my mother how much I appreciate her believing in me for my entire life and for always telling me that anything was possible. I would like to thank my brother Jeremy who I look up to more than anyone. He has always been there when I needed him with the most helpful support. I would like to thank Lee Cohn for being a support for my mother and for helping me through many years of my college. I would like to thank my father, the most brilliant man I know, for his guidance and for always having the answers to any question. I would like to thank Leigh for being the best thing that has ever happen to my father. In addition I would like to thank my brother Steven who has inspired me by his bravery.

I am very thankful to Hugh Herr and the people at the Concord Field Station for there help with the lift measurements. I very much appreciate Randy Pflueger and Dr. Luis Martins, for being subjects for the lift experiments. Their time and insight was critical to this thesis.

I appreciate the patience and support of my close friends, Edward Glicken, Daniel Sobek, Chistopher Scott Jones, Adam Simha, Gus Rancatore, Mark Lubratt, Lee Wienstien and Corine Bickley.

I would also like to thank, Edward Lanzilotta, Mark West, Dr. Jahng Park, Booho Yang, Dr. Sheng Liu, Sooyong Lee, Daniel Braunstein, Xiangdong He, Emile Chamas, Shih-hung Li, Nathan Delson, Nicholas Patrick, David Schloerb, Sudhendu Rai, Anton Pil,

Noriyuki Fujiwara, Samir Nafeh, Susan Ipri and everybody else in Prof. Asada's lab for always answering my question with patience.

There are many others at MIT that have help me to finish this thesis over the years that I would like to thank: Eric Vaaler, Prof. William Durfee, Prof. Sheridan, Prof Amar Bose, Leaslie Regan, Sabina Rataj, Veronica Culbert, Joseph (Tiny) Caloggerio, Norm Mac Askill and Bob Nuttal.

I would also like to thank two outstanding professors that I had at Eastern Illinois University: Prof. William Cloud and Prof. Elan Keiter. Another teacher I appreciated was Mr. Heopner at Niles West who gave me a ground point from which to work up from.

I appreciated the fine work of John & Hubert form J&H Precision for machining the parts of my robot.

I would like to give a special thanks to Rick Tivers for teaching me how to help myself attain my goals.

This Thesis Is Dedicated to My Mom, *Thank you!*

Contents

Chapter 1
Introduction

1.1 Background

Robots are now commonplace in many manufacturing facilities and are becoming more prevalent in construction sites and unstructured environments. One of the major limitations of today's robots, however, is the heavy hardware needed for operation. Specifically, robots require large motors, powerful amplifiers and solid bases to create moderate forces. In order to make robots more useful in the growing applications of construction and autonomous tasks, robots need to be lighter and more efficient. These robots should be capable of moving objects and applying large forces without a rigid base.

To create lighter and more efficient robots a new type of robot design and control methodology is needed. In this thesis a new approach to how robots can be made to create forces is presented. This method will use a dynamic technique rather than the traditional quasi-static technique.

The traditional method for a robot to apply a force is in general quasi-static. First the robot attaches its end effector to the object that the force is to be applied. The desired force at the end effector is created by each of the joint actuators producing a constant torque by some specified amount which results in the desired force.

This thesis will present a class of robots that are capable of dynamically creating forces and manipulating objects with small reaction forces. This new class of robots will take advantage of a special redundant configuration which has the ability to produce dynamic forces by accelerating the center of mass independently of the end effector. This special configuration allows energy to be stored in the mass of the robot and then removed through singular configurations of the robot arm. A large force can be borne by the

structure of the robot near a singular configuration reducing the need for large actuator torques.

The development of a dynamic robot of this type will have many benefits. This dynamic technique can be more efficient by taking advantage of peak output of motors and amplifiers to create forces. In the application of applying forces and manipulating objects it is not necessary for the robots base to be solidly connected to ground. For the task of dynamically lifting, a robot can lift objects through weak configurations. It is expected that this new class of robots will lead to many lighter more efficient robot designs.

1.2 Previous Work

Dynamic body motions have been studied extensively in the area of leg locomotion (Raibert, 1986), (Walron, Wang and Bolin 1985). In the manipulation research, the majority of work has been focused on the dynamic motion control of robot end effectors (Vukovratovic, 1978), (Luh, Walker and Paul 1980), (Hollerbach, 1980), (Khatib, 1983). These control methods, however, do not utilize internal body movements purposely.

An issue relevant to internal motion control can be found in the area of redundant manipulators, where the objectives of internal motion control are collision avoidance, geometric task improvements and singularity avoidance (Nakamura and Hanafusa, 1984), (Baillieul, 1985), (Maciejewski and Klien,1985), (Hu and Goldberg, 1992). Redundant robot systems have also been used to take advantage of singularity configurations during quasistatic climbing (Madhani, 1992) Center of mass control methods have been used to avoid tipping for redundant manipulator/vehicle systems (Fukuda, 1992). In free floating space systems, the inherent fixed center of mass was considered for end-effector control (Papadopoulos and Dubowsky, 1990). Redundant robots were used to manipulate objects while minimizing reaction forces by controlling the center of mass to be fixed (Brown, 1990).

In the field of biomechanics, redundant models of the human form have been used to compute forces and torques required for jumping and running motions (Fujii, 1989). Multi-link models were also used to optimize input torques required for a specified end-effector lifting trajectory (Amirouche, 1991). An optimal control and parameter optimization approach was used to predict maximum jumping height for a complex human musculoskeletal model and compared to human subjects (Pandy, 1992). Articulated angle trajectories of human subjects performing lifting tasks were measured and used by a multi-link model to compute inertial and reactive moments and forces at each articulation (Freivalds, 1982), (Gagnon, 1991). Mechanical power outputs during pull movements in clean and jerk weightlifting were measured to compare mean force levels and mean power levels between olympic and junior or college lifters (Funato, 1989). Force plate measurements and electromyograms measuring muscle activity were used to collect data for a variety of athletic activities (including lifting) to make qualitative comparisons between well trained and moderately trained athletes (Carlsoo, 1972). Human motion of complex industrial tasks has been studied to extract expert techniques for robot learning (Asada, 1988).

Trajectory planning for minimum-time end effector positioning based on human motions has been studied, but the center of mass motion was neglected (Lee and Liao, 1988), (Lee and Shih, 1990). Trajectories for a biped locomotive robot were generated using human center of mass motion and neural networks to solve the inverse kinematics to obtain joint positions (Kitamura, 1988).

1.3 The Problem and Approach

Current robot design and control schemes do not take complete advantage of the entire abilities of the actuators and controllers to create forces. This results in heavier and more expensive robots than are necessary. In traditional robotics, creating quasi-static forces and manipulating objects can be accomplished by solving a kinematic problem. In

contrast, a dynamic method is more complex. By coordinating the internal body movements, controlled dynamic forces can be created. This requires a robot with a specific redundant design and mass distribution to be controlled with a dynamic coordination. For example a force can be created by accelerating the center of mass of a robot to some velocity thereby storing some kinetic energy in the mass of the robot. This energy can be transferred to a large impulsive force at an end effector by using the arm of the robot in a singular configuration to decelerate the center of mass.

There are many ways of utilizing internal body movements for performing dynamic tasks. Dynamic tasks can be classified by examining the type of trajectories with which the center of mass and the end effector move during a task. These cases are determined by whether the center of mass is fixed or moving and whether the end effector is fixed or moving. These tasks can be broken down into the three categories:

1) Zero reaction force manipulation. The case of a fixed center of mass and a moving end effector is the task of zero reaction force manipulation. This task allows a robot to manipulate an object with large accelerations with minimal reaction forces produced to the base. This type of manipulation is achieved by controlling the internal body mass to counteract the forces produced by the moving object. Zero reaction force manipulation was covered in Brown and Asada, 1990.
2) Force production to the environment. The robot's center of mass is moved as a function of time, while the end effector is fixed to a point in the robot workspace. This results in a force produced at that point by accelerating the center of mass.
3) Lifting objects. Both the center of mass and the end effector are moved as a function of time. To dynamically lift an object requires complex trajectories of both the center of mass and the end effector.

This coordinated motion of a redundant mechanism to perform dynamic tasks can be observed in nature. By studying the motion of man we find that many tasks such as opening a stuck door, digging in the ground with a shovel, and loosening a bolt with a wrench is a result of dynamically moving our bodies rather than merely moving our arms and legs in a quasi-static manner.

In order for robotics to be able to take advantage of this dynamic scheme many issues need to be addressed. The critical issues covered in this thesis are:

- The design specifications necessary to build and control a robot that efficiently uses the complete abilities of its actuators and amplifiers in creating forces and lifting using a dynamic technique.
- The strategies used to control this type of robot to perform the task of creating forces and lifting objects.

By addressing these issues we will be able to build robots that more effectively utilize their actuators and amplifiers.

1.4 Overview

The approach of this thesis is to utilize a class of redundant robots that embody design elements that allow energy to be stored in the robot mass and then removed as it moves to singular configurations of the robot's limbs. This section will give an overview of the organization of this thesis.

In Chapter 2, the design of a robot model is presented which contains the minimum parameters that are capable of describing the production of dynamic reaction forces. The redundancy criterion is identified which describes the kinematic robot structure that allows independent control of the robots center of mass and end effector. A method is presented for computing the actuator torque trajectories from the motion trajectories of the end effector and centroid motion. Also in Chapter 2 an ideal mass distribution for the planar

case of a robot that meets the redundancy criterion will be computed. This planar case robot will be used as an exemplary robot through out this thesis.

In Chapter 3, a study of human dynamic motion is presented. This motion was studied to gain an understanding of how humans perform dynamic tasks. These measurements will be used to find a plausible class of tractable trajectories to apply to robotic motion. Humans were measured performing two exemplary dynamic tasks. The forces and motions were measured of humans performing the tasks of trying to open a stuck door and lifting objects. The data measured will be analyzed and interpreted to understand the schemes used by humans to perform these dynamic tasks.

In Chapter 4, a method is presented for computing trajectories for our robot design for the tasks of creating forces and lifting objects. A performance index based on the internal temperature of the robots actuators was found. Trajectories are parameterized based on the human motion. By starting with the human trajectories as initial estimates optimal trajectories for our robot are found using the performance index.

In Chapter 5, the design and construction of a prototype robot is described. This robot is used to test the concepts of producing dynamic forces and lifting using a dynamic technique. The theoretic issues for the ideal design features of a planar robot designed specifically to perform dynamic tasks is presented. The construction issues is addressed which include the structure, materials, transmission, bearings, and actuator of our prototype robot.

In Chapter 6, the prototype tests for the dynamic tasks of applying forces and lifting dynamically are presented. Thermistors were placed on the motors and the temperature was measured after each task. The temperature was compared for the task of lifting using a dynamic technique and a comparison technique. The results of these measurements are presented and discussed.

In Chapter 7, a discussion of the performance of the robots simulation is compared to the performance of the robots during experiment is given. Finally, a summary of each chapter and suggestions for future work are provided.

Chapter 2
Class of Robots and Design Features

In this chapter the theoretical basis for robots that produce controlled dynamic forces is established. Design criterion and design features that a robot must contain are found. A method for relating the forces produced quasi-statically and dynamically to a robot's actuator torques is presented. Given a motion trajectory for the end effector and centroid, the inverse kinematics problem is solved. The robot's actuator torques can be computed from the equations of motion, inverse kinematics solution and the mechanical advantage. Design features for an exemplary design of a robot that produces controlled dynamic forces will also be presented.

2.1 A New Class of Robots

In order to make robots more effective in the construction industry a new class of robots is needed. This new class of robots must be well suited at creating large forces and lift heavy objects. For many tasks it is necessary to pull on objects that are stuck in place, such as, pulling plywood formers off of concrete forms or freeing loose rock from exploded tunnels. For these tasks it is necessary for the robot's end effector to remain in control of the object while the force is being applied. This aspect allows the robot to control the motion of the object after it breaks free. This new class of robots should also be able to lift heavy objects, such as lifting ceiling panels into place. This task also requires that the end effector have control of the object while a force is being applied.

In addition to being able to apply forces and lift heavy objects, these robots should also be light and fast. To use robots in the construction of tall buildings requires that the robots be light and not have large reaction forces since the floors of these building are not designed to handle heavy machinery. Another important aspect in construction is time. The faster a robot can accomplish a task the less the task will cost. With these aspects in mind we will state the goal.

The Goal: Design a robot and control methodology that allows a robot to perform tasks quickly that require large forces while maintaining end effector mobility control. This method should also utilizing the robots weight and actuators very efficiently.

2.2 Examine Options

We begin our search for a new class of robots by examining a simple example. We look at four cases that address the design issues that are used to define our class of robots.

Case 1) Shown in figure 2.1 is a one dimension, one degree of freedom robot applying a force using a traditional quasi-static approach.

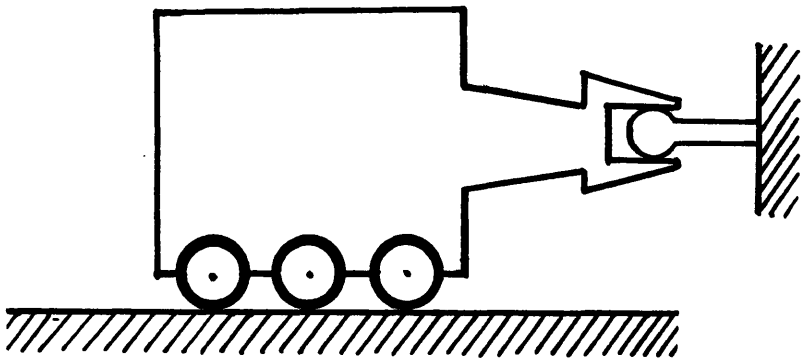

Fig. 2.1: One dimensional single degree of freedom

For this robot to create a force to a fixed object its actuators are turned on and the robot begins to pull using stall torque to produce a quasi-static force. If the object were to

break free the robot could remain in control of the object by shifting its control strategy (bring the object to rest). The force in this case is directly limited by the actuators.

Case 2) One way to get a greater force capability is to use a dynamic approach. Figure 2.2 shows a one dimensional robot that uses an impact method to produce forces.

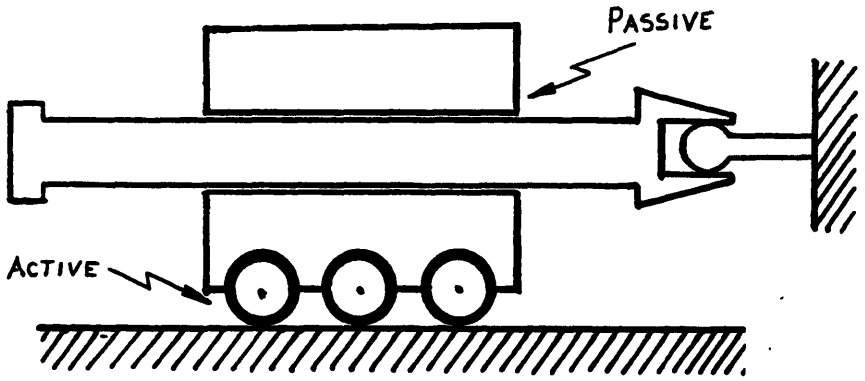

Fig. 2.2: An impact robot

The approach of this design is to accelerate most of the mass of this robot until it reaches a stop that is connected to the end effector. A large force is transferred to the end effector. This force is dependent on the characteristics of the impact (the deceleration of the mass). If the object that the force is being applied to where to break free there would be no way of controlling its motion. This motion may be damaging to the robot or other things nearby.

Case 3) By actuating the passive bearing in Figure 2.2 it would be possible for the end effector to remain in control of the end effector. Dynamic force could be produced by accelerating the mass away from the end effector and using the sliding actuator as a break. This actuator would also allow a more controlled deceleration which provides a more controlled production of force. The duration and magnitude of the force could be varied depending on the breaking characteristics of the sliding actuator. Using this actuated version of figure 2.2 it is possible to create forces for greater durations. The sliding actuator could also be used, in addition to the other actuator, to initially accelerate the

mass. Following this acceleration the sliding actuator would be used to decelerate the mass of the robot and apply the force. In this case the sliding actuator needs to provide a breaking force equal to the applied force. For this reason this case does not provide a benefit.

Case 4) To gain a mechanical advantage we can use a actuated link mechanism instead of a sliding actuator. Figure 2.3 shows our one dimensional two degree of freedom robot with actuated link mechanism.

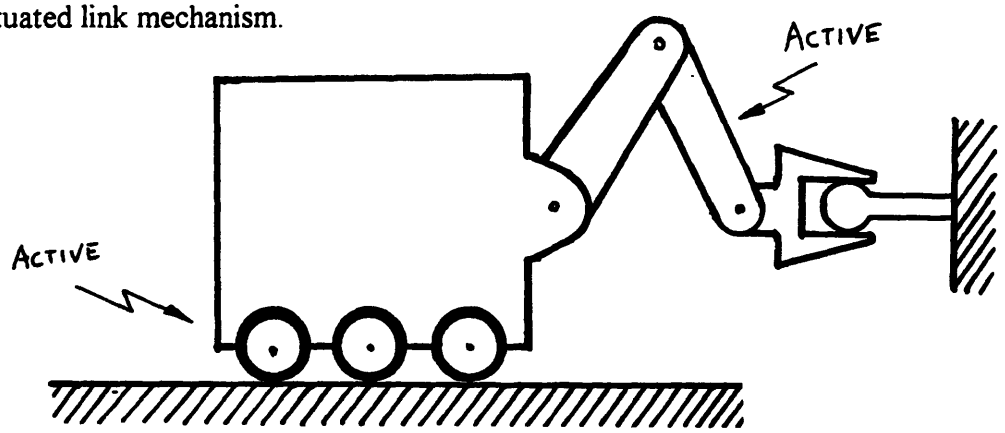

Fig. 2.3: One dimensional, two degree of freedom robot with revolute arm

In this example the robot can still use both actuated systems to accelerate the mass but now the deceleration can be controlled around the singularity of the links. As the links approach an singularity the actuators become more effective at producing high forces since the structure is bearing more of the load. It is this form of a robot that we use to base the class of robots that is studied in this thesis.

We begin our analysis by defining a robot to be series of servoed links, each link having some mass and rotational inertia. A robot will have n degrees of freedom and operate in a m dimensional space.

2.3 Dynamically Produced Reaction Forces

We begin by examining all of the forces and moments that act on each link of a robot with n rigid link connected by servoed joints. Figure 2.4 shows the forces and moments acting

on an arbitrary link (Asada and Slotine, 1986). The equations that govern the forces and moments acting on each link can be written.

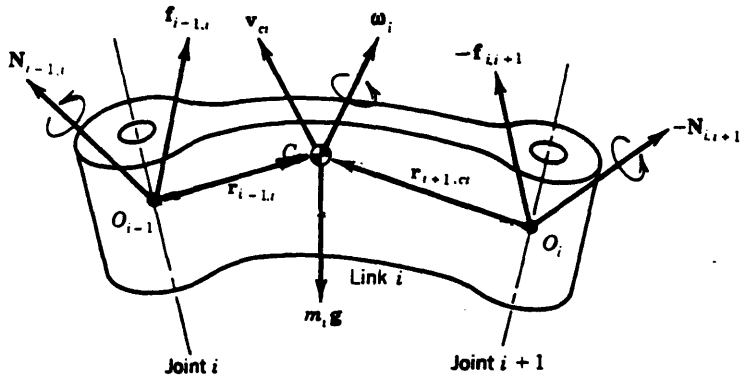

Fig. 2.4: Forces and moments acting on link i

The balance of linear forces can be written

$$\frac{d}{dt}(m_i \mathbf{v}_{ci}) = \mathbf{f}_{i,i-1} - \mathbf{f}_{i,i+1} + m_i \mathbf{g}, \qquad i = 1,\ldots,n \tag{2.1}$$

where m_i is the mass of each link, $\mathbf{v}_{ci}$ is the velocity of the center of mass of each link, $f_{i,i-1}$ is the force exerted by link i-1 (the previous link), $f_{i,i+1}$ is the force exerted by link i+1 (the following link), **g** is the gravitational acceleration,

The balance of moments with respect to the centroid C_i is given by

$$\frac{d}{dt}(\mathbf{I}_i \omega_i) = \mathbf{N}_{i,i-1} - \mathbf{N}_{i,i+1} + \mathbf{r}_{i-1,ci} \times \mathbf{f}_{i,i-1} - \mathbf{r}_{i+1,ci} \times \mathbf{f}_{i,i+1}, \qquad i = 1,\ldots,n \tag{2.2}$$

where $\mathbf{I}_i$ is moment of inertial of each link, ω_i is the angular velocity of the link, $\mathbf{N}_{i,i-1}$ is the torque exerted by link i-1, $\mathbf{N}_{i,i+1}$ is the torque exerted by link i+1, $r_{i-1,ci}$ is the position vector of the center of mass from i-1 joint, and $r_{i+1,ci}$ is the position vector of the center of mass from i+1 joint.

Consider the entire robot. We can write the position of the mass centroid as

$$\mathbf{R}_C = \frac{\sum_{i=1}^{n} m_i \mathbf{r}_{0,ci}}{M_C}, \tag{2.3}$$

where $M_C = \sum_{i=1}^{n} m_i$ and M_C is the total mass of the robot.

Figure 2.5 shows the forces and moments acting on the entire robot. The linear forces can be written as

$$\frac{d}{dt}\left(M_C \dot{\mathbf{R}}_C\right) = \mathbf{f}_{0,1} - \mathbf{f}_{n,n+1} + M_C \mathbf{g}, \tag{2.4}$$

where $f_{0,1}$ is the force exerted by the base on the robot and $f_{n,n+1}$ is the force exerted by the end-effector on the robot. The balance of moments of the entire robot can be written

$$\frac{d}{dt}(\mathbf{L}) = \mathbf{N}_{0,1} - \mathbf{N}_{n,n+1} + \mathbf{R}_{0,C} \times \mathbf{f}_{0,1} - \mathbf{R}_{n+1,C} \times \mathbf{f}_{n,n+1} - \sum_{i=1}^{n} (\mathbf{R}_{C,ci} \times m_i \dot{v}_{ci}), \tag{2.5}$$

where $\mathbf{L} = \sum_{i=1}^{n} \mathbf{I}_i \omega_i$ and $\mathbf{N}_{0,1}$ is the torque exerted by the base on the robot, $\mathbf{N}_{n,n+1}$ is the torque exerted by the end effector on the robot, $\mathbf{R}_{n+1,C}$ is the position vector of the mass centroid with respect to the end-effector, and $\mathbf{R}_{C,ci}$ is the position of the center of mass of each link with respect to the robot mass centroid. We observe from these equations that the linear forces at the base and end-effector are dependent upon the total momentum and not on the momentum of individual links.

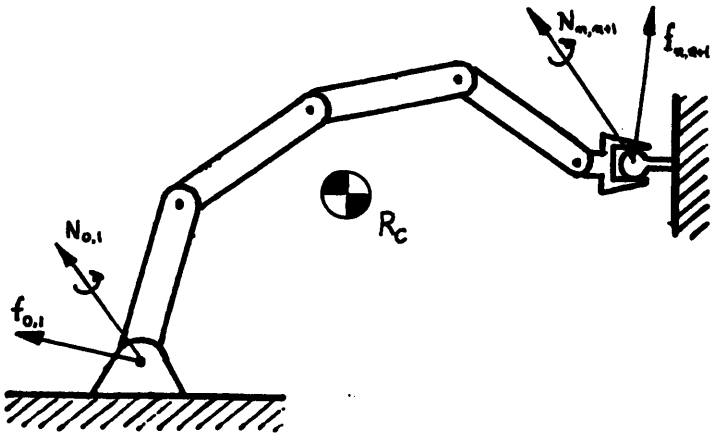

Fig. 2.5: The forces and moments acting on a robot

The dynamic equations of motion of the entire robot can be expressed in terms of the actuator torques. Lagrange's Equations of motion of a n degree of freedom robot can be written

$$\mathbf{H}\ddot{\Theta} + \mathbf{h} = \tau, \tag{2.6}$$

where coefficients **H** and **h** are functions of joint displacements Θ and joint velocities $\dot{\Theta}$.

For all dynamic task performed by our robot, the end-effector's location will be specified with m task coordinates:

$$r_1(t),\ldots,r_m(t). \tag{2.7}$$

Once the end-effector's position is specified there exits (n-m) degrees of freedom which corresponds to the internal body motion shown in Figure 2.6. These remaining degrees of freedom can be represented by (n-m) independent generalized coordinates that satisfy the

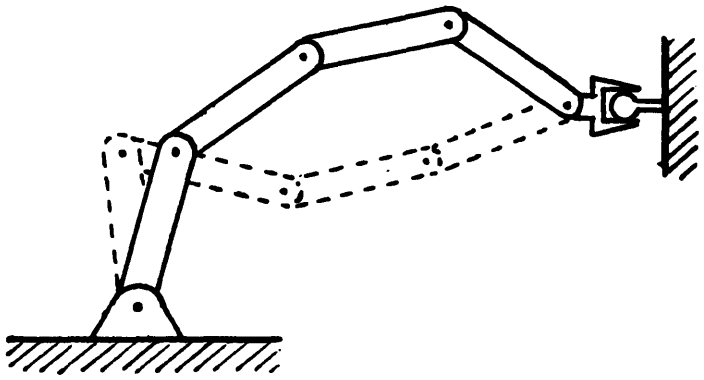

Fig. 2.6: The internal movement of an n-m degree of freedoms

prescribed task coordinates. These generalized coordinate will be represented by

$$\mathbf{q} = (q_1,\ldots,q_{n-m})^T. \tag{2.8}$$

Associated with the generalized coordinates let us specify (n-m) generalized forces that act on the internal body mass (centroid) of the robot. These forces can be represented by

$$\mathbf{Q} = (Q_1,\ldots,Q_{n-m})^T. \tag{2.9}$$

The dynamic equations of the internal body motion can be express as,

$$\mathbf{H}_R\ddot{\mathbf{q}} + \mathbf{h}_R = \mathbf{Q}. \tag{2.10}$$

By moving the internal body, generalized forces **Q** are created. These generalized forces can be related to the robot's actuator torques with

$$\mathbf{Q}=\mathbf{D}\tau, \tag{2.11}$$

where **D** is a $(n\text{-}m)$x n matrix that distributes **Q** to τ.

The forces and moments transmitted to the environment and the base are determined by the distribution of the actuator torques to produce the generalized forces **Q**. **D** will be $(n\text{-}m)xn$ dimensions which is rectangular and infers that the robot must be redundant.

2.4 The Redundancy Criterion

In order for a robot to create arbitrary dynamic forces at its end effector and base the robot must have the ability to move its end effector independently from the center of mass. This ability assumes that our robot will be defined as having the ability to move its end effector to arbitrary positions in its workspace independent of the dynamic forces created. This functionality can be achieved by designing the robot with a special form of redundancy. To be able to move the end effector separately from the center of mass, for each generalized task coordinate m there must be robot mass that can be controlled to move in the same direction or the opposite direction as the end effector. To achieve this criterion the robot should be designed such that for each generalized task coordinate m of the end effector there exists at least two degrees of freedom n. This relationship can be written:

$$n=2m \tag{2.12}$$

2.5 Computing Actuator Torques

For any dynamic task the force $\mathbf{F}_r$ desired at the end-effector will be specified. The torque τ_r needed to bear the force $\mathbf{F}_r$ borne by the structure can be computed from

$$\tau_r = \mathbf{J}^T \mathbf{F}_r, \tag{2.13}$$

where $\mathbf{J}$ is the Jacobian relationship of infinitesimal change in joint angle to endpoint displacement. We can express the total torque needed to bear the force and to account for the dynamic internal motion as

$$\tau = \tau_r + \tau_R,, \tag{2.14}$$

where the internal body dynamics can be represented by Equation 2.10 and τ_R can be computed from

$$\mathbf{Q} = \mathbf{D}\tau_R, \tag{2.15}$$

To find an expression to relate these forces and torques. We examine the velocity relationship between the endpoint velocity and joint angles.

The end-effector velocity (*m* terms) can be represented in terms of the angular joint velocity of the robot using the Jacobian relationship of the robot as

$$\dot{\mathbf{r}} = \mathbf{J}_r \dot{\Theta}. \tag{2.16}$$

The velocity of the mass centroid of the robot (*n-m* terms) can also be represented in terms of the angular joint velocity of the robot using another Jacobian as

$$\dot{\mathbf{R}} = \mathbf{J}_R \dot{\Theta}. \tag{2.17}$$

We can combine the two previous equations into one generalized expression.

$$\begin{bmatrix} \dot{\mathbf{r}} \\ \dot{\mathbf{R}} \end{bmatrix} = \left[\mathbf{J}^*\right]\dot{\Theta}, \qquad (\det \mathbf{J}^* \neq 0) \tag{2.18}$$

where $\mathbf{J}^* = \begin{bmatrix} \mathbf{J}_r \\ \mathbf{J}_R \end{bmatrix}$. The angular joint velocities can be determined in terms of the velocity of the end-effector and velocity of the center of mass:

$$\dot{\Theta} = \mathbf{J}^{*-1} \begin{bmatrix} \dot{\mathbf{r}} \\ \dot{\mathbf{R}} \end{bmatrix} = \left[\hat{\mathbf{J}}_r, \hat{\mathbf{J}}_R\right] \begin{bmatrix} \dot{\mathbf{r}} \\ \dot{\mathbf{R}} \end{bmatrix}, \tag{2.19}$$

where $\hat{\mathbf{J}}_r$ is the inverse Jacobian associated with the end-effector velocity and $\hat{\mathbf{J}}_R$ is the inverse Jacobian associated with the mass centroid velocity. Using the duality principle we can write the force that the end-effector applies and the generalized forces acting on the center of mass as

$$\begin{bmatrix} \mathbf{F}_r \\ \mathbf{Q} \end{bmatrix} = \mathbf{J}^{*-T} \tau_{..} \tag{2.20}$$

If we examine the case of applying forces and assume that the end-effector is fixed $\dot{\mathbf{r}} = 0$. Then the joint angular velocities of the robot can be computed by

$$\dot{\Theta} = \hat{\mathbf{J}}_R \dot{\mathbf{R}}, \tag{2.21}$$

The torque needed by the actuators to apply a force at the end-effector and apply the generalized forces applied to the center of mass can be expressed with the following:

$$\tau = \mathbf{J}_r^T \mathbf{F}_r + \mathbf{J}_R^T Q. \tag{2.22}$$

Using Equations 2.10 and 2.22 the actuator torques needed to move the robot can be determined. The torques $\mathbf{J}^T\mathbf{F}_r$ can be provided not only by the actuators but also by the internal body motion; $\mathbf{J}_r^T\mathbf{F}_r = \tau + \mathbf{J}_R^T Q$.

2.6 Centroid and End Effector Motion

In this section we will develop an analytical way of expressing the position of the end effector and centroid in terms of the joint displacements of our robot. An expression for the position of the end effector can be written as

$$\mathbf{r} = \sum_{k=1}^{n} \mathbf{l}_k, \tag{2.23}$$

where $\mathbf{l}_k$ is the pivot-to-pivot length vector of each link. The position of the end effector can be written in terms of its m components, as

$$\mathbf{r} = [r_1, r_2, \ldots r_m]^T. \tag{2.24}$$

Each of the end effector coordinates can be written as

$$r_j = \mathrm{f}_j(q_1, q_2, \ldots, q_n), \quad j = 1, \ldots, m \tag{2.25}$$

where r_j represents the coordinates of the end effector and the q_i are the joint displacements. The center of mass trajectory can be written (using Tepper and Lowen, 1972 notation) as

$$\mathbf{R} = \frac{1}{M_C} \sum_{j=1}^{n} m_j \mathbf{r}_{Sj}, \tag{2.26}$$

where M_C is the total mass of the robot, m_j is the mass of each link, $\mathbf{r}_{Sj}$ is the position vector of each link.

The center of mass trajectory can be rewritten by expanding the position $\mathbf{r}_{Sj}$ of the center of mass of each link as

$$\mathbf{r}_{Sj} = \mathbf{r}_j + \sum_{k=1}^{j-1} \mathbf{l}_k \tag{2.27}$$

and substituting this expression into equation (2.26) to give

$$\mathbf{R} = \frac{1}{M_C} \sum_{j=1}^{n} \left\{ m_j \left[\mathbf{r}_j + \sum_{k=1}^{j-1} \mathbf{l}_k \right] \right\}. \tag{2.28}$$

That is, for each link in a mechanism, a trajectory vector can be found that is represented by the sum of the pivot-to-pivot length vectors ($\mathbf{l}_k$) and the center of mass vectors ($\mathbf{r}_j$) that define the distance from the end of a link to its center of mass. By multiplying each of these vectors by the mass of each link m_j, summing them together, and then dividing by the total mass M_C, an expression for the center of mass $\mathbf{R}$ can be found.

The position of the center of mass can be written in terms of its m components as

$$\mathbf{R} = [R_1, R_2, \ldots R_m]^T. \tag{2.29}$$

These components are also a function of the n joint displacements

$$R_j = g_j(q_1, q_2, \ldots, q_n), \; j = 1, \ldots, m \tag{2.30}$$

where the coordinates R_j represent the center of mass position.

2.7 Inverse Kinematics

In this section we present a method for determining the joint displacements in terms of end effector and center of mass positions. In the previous section we found the end effector and centroid position in terms of the joint displacements. By meeting the redundancy criterion we have m coordinates for the end effector and n-m coordinates for the centroid and n joint generalized coordinates which would be equal to $2m$ if the redundancy criterion was satisfied for a planar robot with two internal body degrees of freedom.

Therefore there are n equations and n unknowns. Let us represent the joint displacements $q_1,\ldots,q_n$ that satisfy both equations (2.25) and (2.30) as functions of r_i and R_i. Namely,

$$q_i = h_i(r_1,\ldots,r_m,R_1,\ldots,R_m), \qquad i = 1,\ldots,n. \tag{2.31}$$

If there exists a closed-form solution, this solution would give us absolute joint displacements for given positions of the end effector and center of mass.

Because of the form of Equations (2.25) and (2.30), it may not always be possible to find a closed form solution even though the system will always have n equations and n unknowns. For the cases in which a closed form solution for the joint displacements does not exist, numerical methods can be applied to calculate the joint positions.

Equation (2.30) gives the expression for the joint positions in terms of the centroid and end effector positions. To convert the time trajectory of the end-effector and centroid into joint position trajectories the end effector and centroid trajectories can be discretized into a number of positions and using Equation 2.31 a unique configuration of the robot could be computed for each of these positions.

In the following section we use the expression for the position of the end effector and centroid to find an ideal mass distribution for an exemplary robot. In this thesis we will examine the case of planar motion. To meet the redundancy criterion a four degree of freedom robot is needed. A serial chain of four links is selected for the design of our robot.

2.8 An Exemplary Robot Model

We would like to design our dynamic robot so that the center of mass is able to be controlled independently from the end effector. To begin with we examine a general mass distribution form of the serial four degree of freedom robot. For this robot shown in Figure 2.7, we can write the equations for the end effector using Equation (2.25):

$$x = \sum_{i=1}^{4} l_i \cos\theta_i \tag{2.32}$$

and

$$y = \sum_{i=1}^{4} l_i \sin\theta_i, \tag{2.33}$$

where x and y are the positions of the end effector, each l_i is the length of each link, and θ_i are the joint displacements. We would also like to control the center of mass of our robot. Using Equation 2.30 we will define the positions of the center of mass:

$$X = \sum_{i=1}^{4} A_i \cos\theta_i \tag{2.34}$$

and

$$Y = \sum_{i=1}^{4} A_i \sin\theta_i, \tag{2.35}$$

where X and Y are the positions of the center of mass and the A_i are constants that

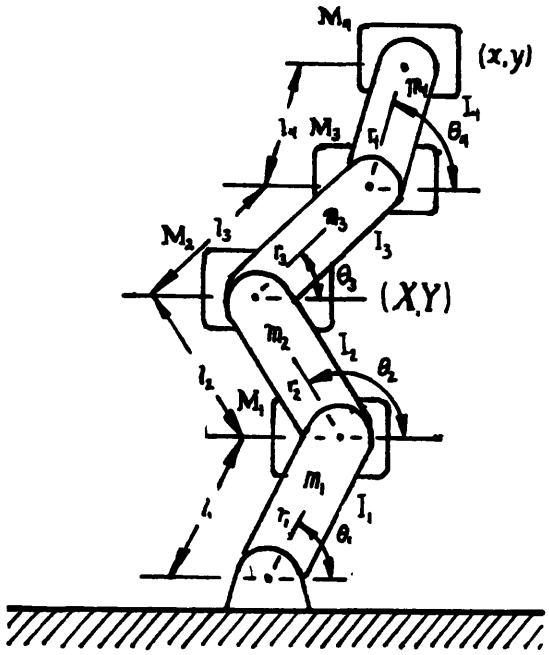

Figure 2.7: General mass distribution form of 4 d.o.f. robot.

contain the mass and dimensional properties and are defined as

$$A_i = \frac{1}{M_T}\left\{ m_i r_i + l_i \left[\sum_{j=i}^{n} M_j + \sum_{k=i+1}^{n} m_k \right] \right\}, \qquad i = 1,\ldots,n$$

If we design our robot with most of the mass at M_2 then $A_1 \approx l_1, A_2 \approx l_2, A_3 \approx 0$, and $A_4 \approx 0$ and our equation for the center of mass position reduces to:

$$X = l_1 \cos\theta_1 + l_2 \cos\theta_2 \tag{2.36}$$

and

$$Y = l_1 \sin\theta_1 + l_2 \sin\theta_2. \tag{2.37}$$

Now the center of mass equations have two unknowns and is directly solvable. By placing all or most of the mass in the M_2 position the problem of controlling the robots center of mass becomes a simple one.

For the rest of this thesis we will use this exemplary robot model. We will assume all of the links are mass-less. The links from the base to the mass M_2 will be referred to as the leg and links from M_2 to the end-effector will be referred to as the arm. Since most of the mass is located at M_2 for this model this position will be referred to as the centroid of the robot. Figure 2.8 show a diagram of the exemplary robot model considered in this thesis.

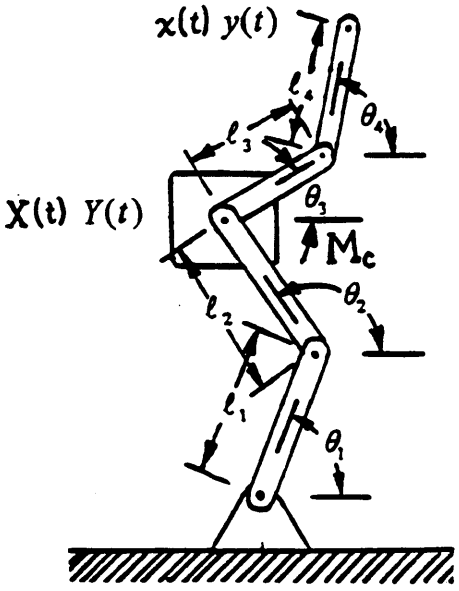

Fig. 2.8: Exemplary 4 degree of freedom robot

The centroid coordinates X, Y can be used as independent generalized coordinates for distributing the internal body dynamics:

$$M_C\ddot{\mathbf{R}} + M_C\mathbf{g} = \mathbf{Q}, \tag{2.38}$$

where $\mathbf{Q}$ are the generalized forces acting on the centroid which can be related to the actuator torques with the $\mathbf{D}$ matrix with Equation 2.15. The actuator torques for this example can be expressed as

$$\tau = (\tau_1, \tau\ , \tau_3, \tau_4)^T. \tag{2.39}$$

The generalized forces acting on the centroid can be expressed in terms of its components:

$$\mathbf{Q} = (F_{Rx}, F_{Ry})^T. \tag{2.40}$$

The velocity of the centroid can be written in terms of the joint velocities of the leg using the Jacobian relationship:

$$\dot{\mathbf{R}} = \mathbf{J}_L\dot{\Theta}_L, \qquad \text{where } \Theta_L = (\theta_1, \theta_2)^T. \tag{2.41}$$

The velocity of the end effector can also be written

$$\dot{\mathbf{r}} = \dot{\mathbf{R}} + \mathbf{J}_A\dot{\Theta}_A, \qquad \text{where } \Theta_A = (\theta_3, \theta_4)^T. \tag{2.42}$$

If we consider the task of applying forces, the end-effector velocity would be set to zero and the centroid velocity could be written in terms of the arm joint velocities:

$$\dot{\mathbf{R}} = -\mathbf{J}_A\dot{\Theta}_A,. \tag{2.43}$$

Using the duality principle we can write the quasi-static forces borne by the robot in terms of the actuator torques. The forces produced on the centroid due to the leg actuator torques can be expressed as

$$\tau_L = \mathbf{J}_L^T\mathbf{F}_L, \qquad \text{where } \tau_L = (\tau_1, \tau_2)^T. \tag{2.44}$$

The forces produced on the centroid due to the arm can also be written

$$\tau_A = -\mathbf{J}_A^T\mathbf{F}_A, \qquad \text{where } \tau_A = (\tau_3, \tau_4)^T. \tag{2.45}$$

The total generalized forces acting on the centroid are the sum of the forces produced by the arm and the leg which can be written

$$\mathbf{Q} = \mathbf{F}_L + \mathbf{F}_A. \tag{2.46}$$

Figure 2.9 shows the forces produced by the arm and leg acting on the robot centroid.

For non-singular configurations the force produced on the centroid by the leg can be written in terms of the leg torques $\mathbf{F}_L = \mathbf{J}_L^{-T}\tau_L$. The forces produced by the arm on the centroid can be written in terms of the arm torques $\mathbf{F}_A = -\mathbf{J}_A^{-T}\tau_A$. The **D** matrix, which relates the torques to the generalized forces ($\mathbf{Q} = \mathbf{D}\tau$) can be written

$$\mathbf{D} = [\mathbf{J}_L^{-T}, -\mathbf{J}_A^{-T}]. \tag{2.47}$$

For our example the **D** matrix has dimensions 2x4. It is possible for the leg or the arm to create the same force on the centroid. For each dynamic task the force created to the centroid needs to be distributed between the leg and the arm. To determine how these forces can be effectively distributed we examine the mechanical advantage.

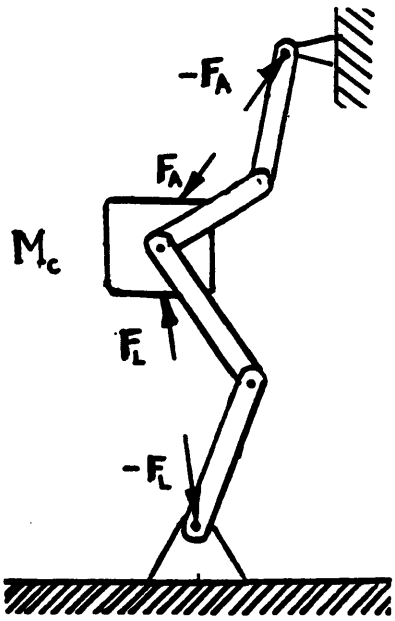

Fig. 2.9 Forces acting on robot centroid

2.9 The Mechanical Advantage

We can represent the mechanical advantage by defining a transformer ratio that relates the input torque to the force borne by the robot (Asada and Cro-Granito, 1985). We can write this ratio as

$$A = \frac{|\mathbf{F}|}{|\tau|}, \tag{2.48}$$

where A is the mechanical advantage. To find our mechanical advantage in terms of the vector quantities we can compute the square of A. By substituting the torque/force relationship $\tau = \mathbf{J}^T\mathbf{F}$ into Equation 2.48, we can find the mechanical advantage in terms of the force and the jacobian matrix:

$$A^2 = \frac{\mathbf{F}^T\mathbf{F}}{\tau^T\tau} = \frac{\mathbf{F}^T\mathbf{F}}{\mathbf{F}^T\mathbf{J}\mathbf{J}^T\mathbf{F}}. \tag{2.49}$$

The mechanical advantage varies depending on the direction of **F**. The maximum and minimum are provided by solving the eigenvalue problem.

$$\mathbf{J}\mathbf{J}^T\mathbf{F} = \lambda\mathbf{F}, \tag{2.50}$$

where λ is the eigenvalue of matrix $\mathbf{J}\mathbf{J}^T$. Solving Equation 2.50 for λ and plugging into Equation 2.49 our mechanical advantage will be

$$A = \frac{1}{\sqrt{\lambda}}, \tag{2.51}$$

where the largest eigenvalue is the smallest mechanical advantage in the direction of the corresponding to the eigenvector and the smallest eigenvalue corresponding to the largest mechanical advantage:

$$\frac{1}{\sqrt{\lambda_{max}}} \le A \le \frac{1}{\sqrt{\lambda_{min}}}. \tag{2.52}$$

By assuming a constant power input this mechanical advantage can be represented by an ellipsoid. Where the largest eigenvalue corresponds to the minor axis and the smallest corresponds to the major axis. Figure 2.10 shows an example of a two dimensional robot in two configurations with an ellipsoid showing the direction of largest mechanical advantage.

The trajectory of the centroid and end effector can be derived using a combination of the previous sections. In Chapter 4 we compute an optimized trajectory using human motion as an initial estimate. Position trajectories can be computed by specifying the initial and

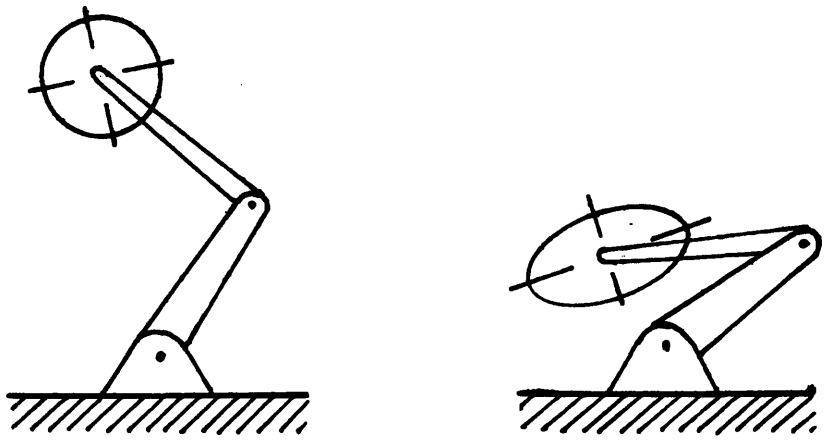

Fig. 2.10 The mechanical advantage of a two degree of freedom robot

final conditions on the motion of the centroid and end effector trajectories. Since there are an infinite number of initial and final conditions possible, human motion was studied in Chapter 3 to understand how humans take advantage of these conditions. Assuming that a trajectory can be computed for the motion of the centroid we will find expressions of how to relate this motion into joint displacements and finally, actuator torques.

2.10 The Human Form

The human body has many redundant degrees of freedom. This allows humans to be very flexible in accomplishing many tasks. Examining the horizontal plane of the human form, we find that the human motion in this plane can be modeled as a planar, four degrees of freedom series of links, with most of the body mass located between the arm and leg.

The robot we have designed can model the human form in the vertical plane observed from the side. By making this analogy it is possible to learn how to perform dynamic tasks by examining human motion.

In the following chapter human measurement is presented. Humans are measured performing two dynamic tasks, applying forces and dynamic lifting. By taking advantage of our model we can simplify the measurement of this complex motion. We will limit our interest to only measuring the forces created at the base and end effector and the motion trajectories of the center of mass and end effector.

Chapter 3
Dynamic Force Generation

In this chapter human dynamic motion was studied to gain an understanding of how humans perform dynamic tasks. These measurements will be used to extract relevant schemes and to apply this knowledge to robotic motion. Humans were measured performing two exemplary dynamic tasks. We assumed a simple model of the human to explain forces production for these dynamic tasks. The human was modeled as a two dimensional string of n mass less links with the human's body mass located in the middle of the chain of links. Considering this model we were interested in measuring the position trajectories of only the humans center of mass and end effector. Also of interest was the forces produced through the end effector and the humans feet. These data of interest were measured for both tasks. This data measured will be analyzed and interpreted to understand the schemes used by humans to perform these dynamic tasks.

3.1 Human Production of Force

Human dynamic motion was studied in order to understand the physics of dynamic task performance, in this section an exemplary task of applying forces is considered, and critical features of human task strategies will be obtained from this example. Figure 3.1 shows the simple task of opening a heavy door. As we experienced, we utilize the counteraction of the body motion to generate a large force. Namely, first we push the body away from the door, and keep increasing the momentum in that direction (Fig. 3.1-a). This continues until the arm is nearly extended (Fig. 3.1-b). At the time of full arm extension, which is a singular configuration of the arm, the body momentum is decreased abruptly, creating an enormous pulling force at the door knob. The forces generated

dynamically as in this exemplary task are significantly larger than the ones generated statically, that is, the force created without large momentum changes.

It is highly desirable to understand how a human is capable of producing dynamic forces and to study human dynamic motion so we can apply this knowledge to determining trajectories for a robot that is capable of a similar dynamic motion.

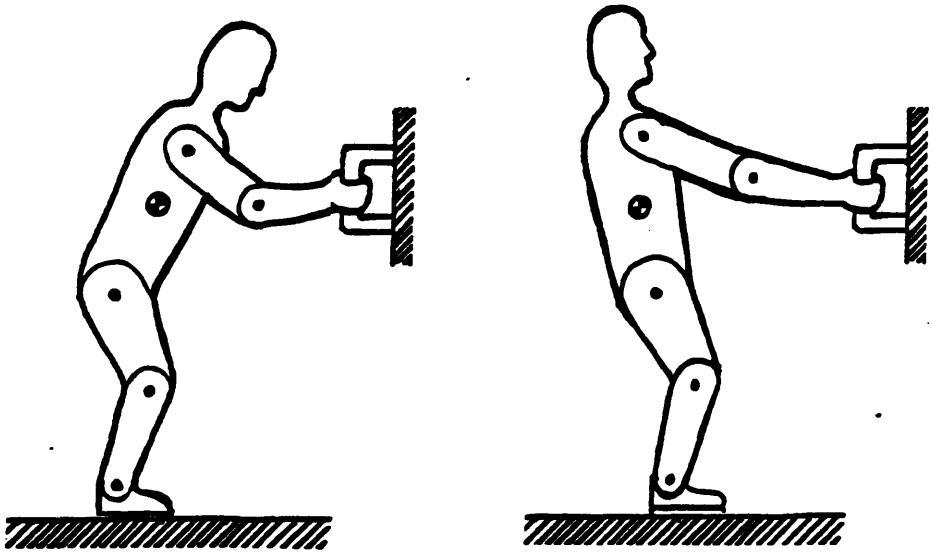

a) b)

Figure 3.1: Human door opening task

3.2 Measurement of Human Dynamic Force

3.2.1 Experimental Setup

To measure dynamic forces produced by humans an experiment of opening a stuck door was chosen. The experiment was performed using a door that was instrumented with a force sensing handle. This door was secured shut during the experiment. Horizontal forces on the floor were measured using a force sensing floor tile. Nine subjects participated in the experiment. Each subject was asked to stand on the force tile, to hold on to the door handle, and on cue (when sampling was initiated) to pull as hard as

possible with a constant force for three seconds, then to pause, and then to apply as high a force as possible using any means. Data were collected for 10 seconds for each subject. A 20 Hz sampling rate was used to collect the forces measured. To measure the motion of the subjects approximate center of mass, each subject was recorded from the side with a video camera.

3.2.2 Results

Figure 3.2 and 3.3 show typical results of the force measurements collected. The upper line is the measured force applied to the door handle. The lower line shows the force measured from the floor tile sensor. Positive force indicate a force in a direction away from the door (parallel to the floor). The initial (3 second) quasi-static part of the force data can be seen as the mirror image forces shown in figure 3.2 the

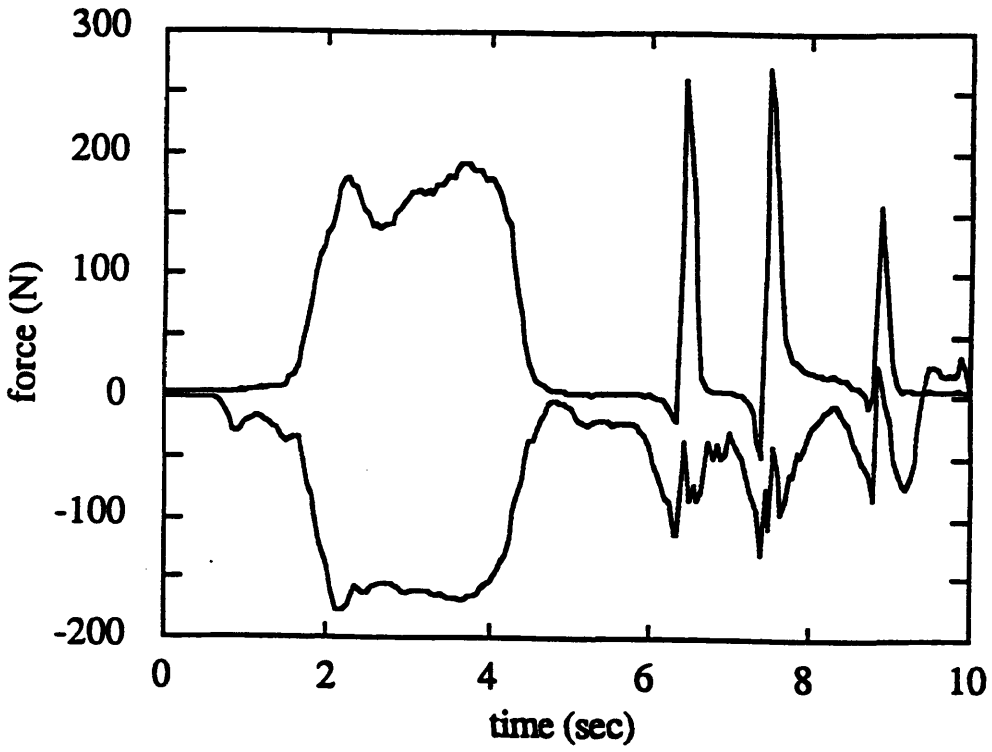

Figure 3.2: Force measured for subject 1

second part of the force measurements can be seen as a repeating pattern of peak forces. Each pattern begins with a small force which can be seen in Figure 3.2 labeled f1 and then

a large force created to the door handle labeled h1 followed by another small force labeled f2. Figure 3.3 also exhibits similar patterns.

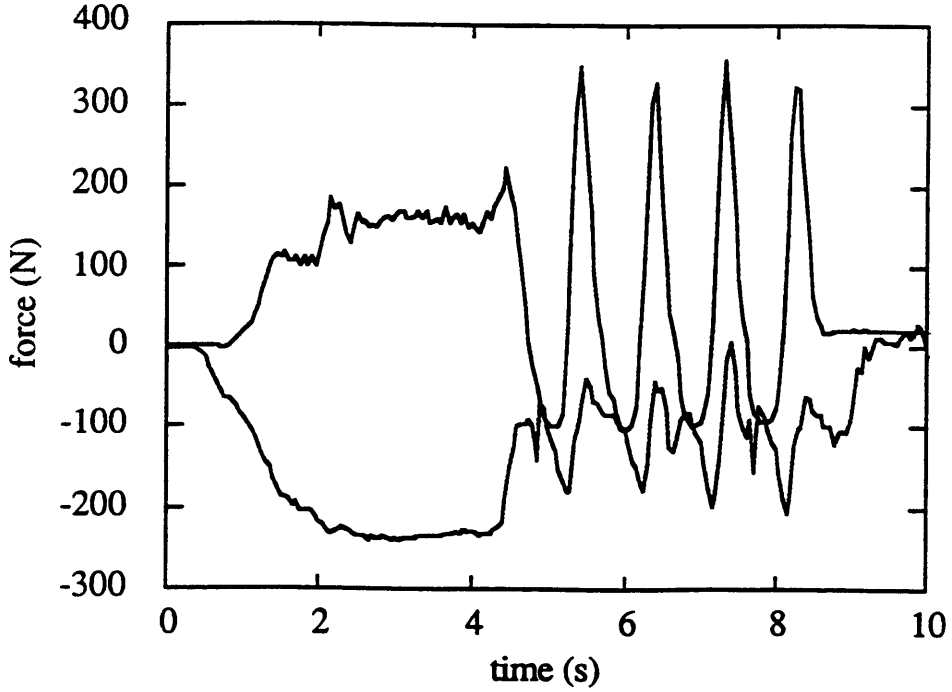

Figure 3.3: Force measured for subject 2

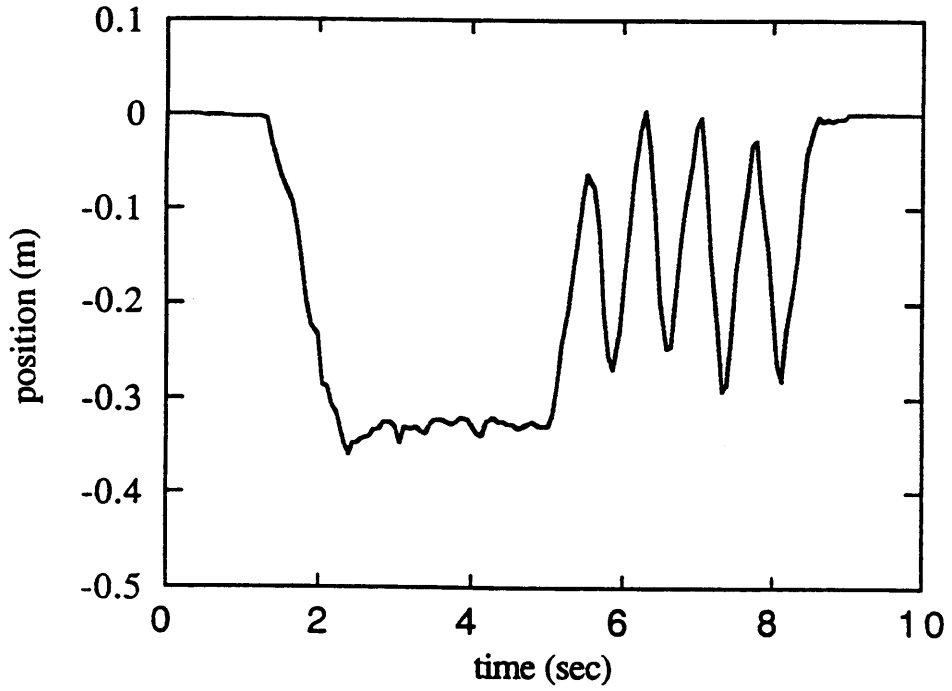

Figure 3.4: Position measured for subject 2

The video tape of the subject motion was digitized using a software package called Image. The results of this digitization are shown in Figure 3.4. The graph shows the horizontal displacement of the subject's approximate center of mass. Zero is defined by the initial starting position of the subject's motion.

3.2.3 Discussion

During the initial quasi-static phase of the measurements an expected mirror image force on the floor and door in both Figures 3.2 and 3.3 can be seen. After the short pause the second phase of the force production can be seen. In each case the subject always resorted to a dynamic method for the second phase of the sampling period. Several dynamic force attempts can be seen applied to the door. For each of these dynamic forces a pattern of forces on the door and on the floor can be seen. The beginning of each dynamic force begins with a force pushing on the floor tile toward the door. This force can be seen in Fig. 3.2 (labeled f1). The push on the tile is created by the subjects legs pushing their body away from the door, accelerating their body mass. As the subjects arm approaches a completely extended configuration (a singular configuration), the subjects body is decelerated rapidly with only a relatively small torque required by the subject's arm muscles. This deceleration results in a large force borne through the subjects arm to the door handle. This force can be seen as h1 in Figure 3.2. This large force is exerted for the time of the subjects body being decelerated, while the arm is near its extended singularity. After this force has been created a recovery force labeled f2 exerted by the legs of the subject decelerates the subjects body back to rest at the starting position. The body is now in a configuration to repeat the task.

The peak force produced to the door during the dynamic phase is 50% greater than the peak force produced during the quasi-static phase. In addition, the initial pushing forces and recovery forces produced to the floor are 45% less than the forces on the floor created during the quasi-static phase. This demonstrates the ability for a human to direct forces. Directing forces could be an important tool in the field of robotics and shows the need to understand this dynamic method.

Figure 3.4 shows the motion of subject 2's body This motion shows the acceleration and deceleration of the subject approximate centroid. This motion can be seen to be held constant for the quasi static phase and shown to oscillate for the dynamic phase. It is this oscillating motion that permits the dynamic case to produce large forces.

The door opening task is a simple example since the end-effector is fixed in space. Humans can perform much more complex tasks by utilizing the whole body dynamically and effectively. In the following sections we will focus on weight lifting as an exemplary task.

3.3 Analysis of Weight Lifting Athletes Using Dynamic Lift

Trained athletes are capable of lifting as much as three and a half times their weight to a position over their head very quickly. This is possible by using the so-called "dynamic lifting technique" in which the whole body motion is precisely coordinated with the barbell motion.

Figure 3.5 shows the basic form of the 'power clean' lift. The human subject begins with his knees bent in a crouched position shown by configuration c1. The mass is lifted with a moderate force until the

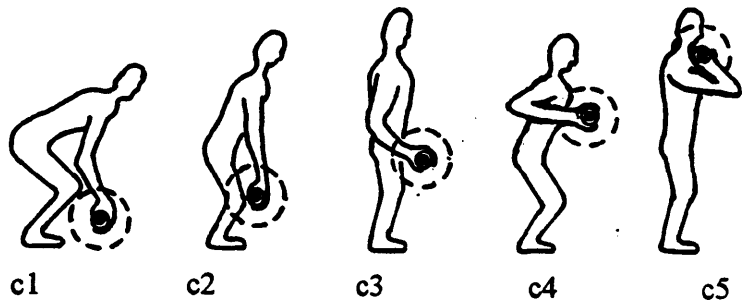

Figure 3.5: The 'power clean' dynamic lift

mass reaches the knees (c2). After this point, the greatest force is applied to the mass. This pull is accomplished by the subject's back thrusting backward and legs thrusting the

body upward. The mass is pulled up by the arms, which at this time are fully extended (acting as ropes connected to the shoulders). This thrust can be large enough for the subject and the mass to become airborne. The subject, while airborne, continues to pull on the mass (c3). This pulling causes the mass to continue moving upward and brings the lifter back in contact with the ground. After reaching this point, the lifter is no longer able to apply a substantial force to the bar because of the configuration of his arms. Although no large force is applied, the bar continues moving upward as a projectile and approaches the top of its trajectory. During this time the subject bends his knees, dipping to a semi-squat, and positions himself under the mass (c4). The mass then comes to rest on the subject's chest, with his arms in a completely bent configuration. The subject then pushes himself and the mass upward with his legs until the subject is standing with the mass at his chest (c5). In weight lifting competition the lifter would then produce the 'jerk' part of the lift which is the push of the weight above the lifters head. For our experiment only the 'power clean' part of the lift will be measured and analyzed.

3.4 Measurement of Athletes' Lifting Motion

3.4.1 Experimental Setup

As shown in Figure 3.6, the subjects stood on a force plate to measure the forces between the subjects body and the floor, and the bar was instrumented with a force sensor to measure the forces between the subject's body and the lifted mass. Two video cameras were used to record the motion of the subject. One was placed directly in front of the lifter and the other was placed on the side of the lifter. The subject's motion was recorded from the front with a high speed (200 frames/sec) video camera placed 23 feet from the subject. The side motion was recorded using a normal speed (30 frames/sec) video camera placed 20 feet from the subjects. Markers were placed on the joints and approximate centroid of the subject's body as well as on the lifted mass. Sampling of force information was done using data acquisition software, Lab View, on a Macintosh IIci with a sampling rate of 200 Hz. The subject informed us when he was ready and then the motion was recorded for five seconds. At the beginning of the sampling period a photo

sensor was tripped in the view of both video cameras and the signal was recorded by the computer. This action was done so that the video and force data could be synchronized during analysis.

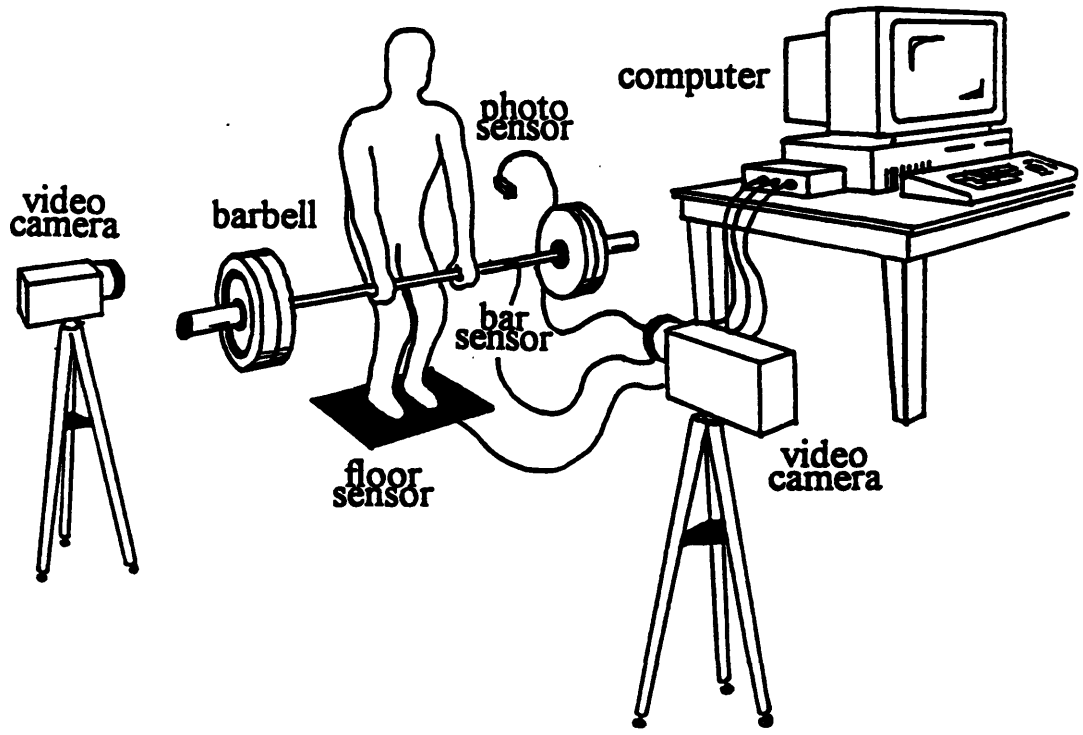

Figure 3.6: Experimental setup

3.4.2 Results

Figure 3.7 shows the time profile of the force measurements taken during a 205 lbs 'power clean'. For comparison purposes the forces on the floor has been inverted and subject A's weight has been subtracted. Notice the two first peaks marked p1 and p2 respectively and the dip between these peaks marked d1. Following d1 there is a small dip d2 that occurs on the bar at the same time as p2. After this small dip there is a small peak force p3 produce on the bar. This detail is followed by a large drop in force on the floor marked d3, followed by the drop of force on the bar marked d4. After these drops there is a large sharp force on the floor labeled p4 followed by another peak force on the bar labeled p5. These peaks are followed by oscillations and another drop in forces at d5

followed by a peak force p6, although in this case the force on the floor and the force on the bar are occurring approximately in phase.

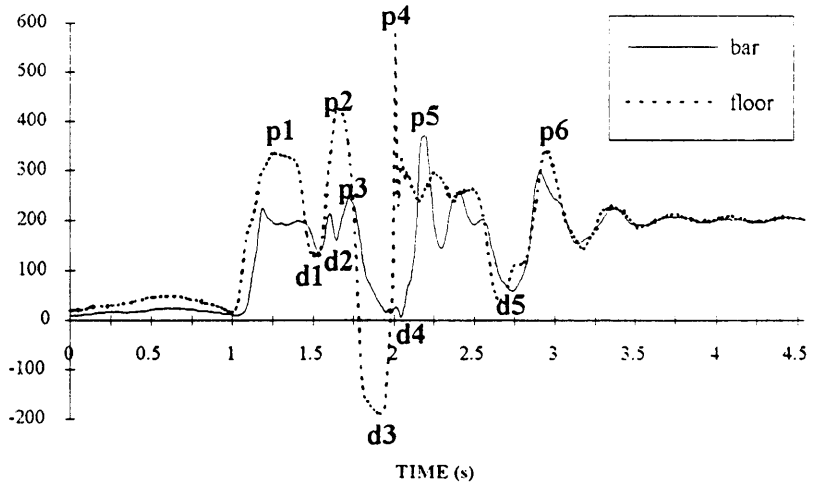

Figure 3.7: Forces measured during subject A's lift

Figure 3.8 shows the force profile during a 225 lbs 'power clean' by subject B. Again for comparison purposes the force on the floor has been inverted and subject B's weight has been subtracted. It is apparent that both of these subjects have relatively the same signature force curves for this lift with deviations in the magnitude of the peaks.

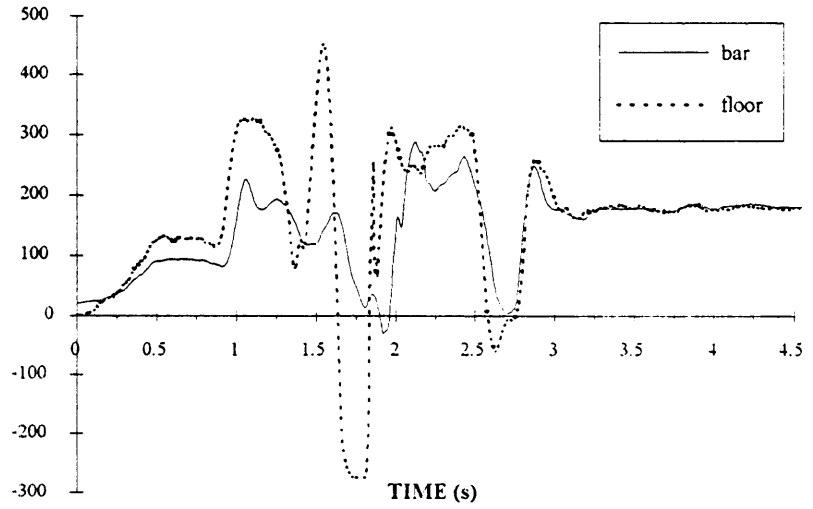

Figure 3.8: Forces measured during subject B's lift

Figure 3.8 shows the force profile during a 225 lbs 'power clean' by subject B. Again for comparison purposes the force on the floor has been inverted and subject B's weight has been subtracted. It is apparent that both of these subjects have relatively the same signature force curves for this lift with deviations in the magnitude of the peaks.

The side view of subject A's lift was digitized using a software package called Image. The results of this digitization are shown in Figure 3.9. The graph shows the vertical displacement of the bar and subject A's approximate center of mass. There is a small flat spot in the trajectory of the bar labeled stall point.

Another feature to notice is the peak of the subjects centroid as the bar continues to move upward. After this peak the trajectory of the centroid and the bar move almost in unison.

3.4.3 Discussion

The patterns in the graph of measured forces provide useful information as to how a person lifts dynamically. If we examine Subject A's lift in Figure 3.7 we find a distinct pattern that Subject A repeated every time he lifted during the experiment.

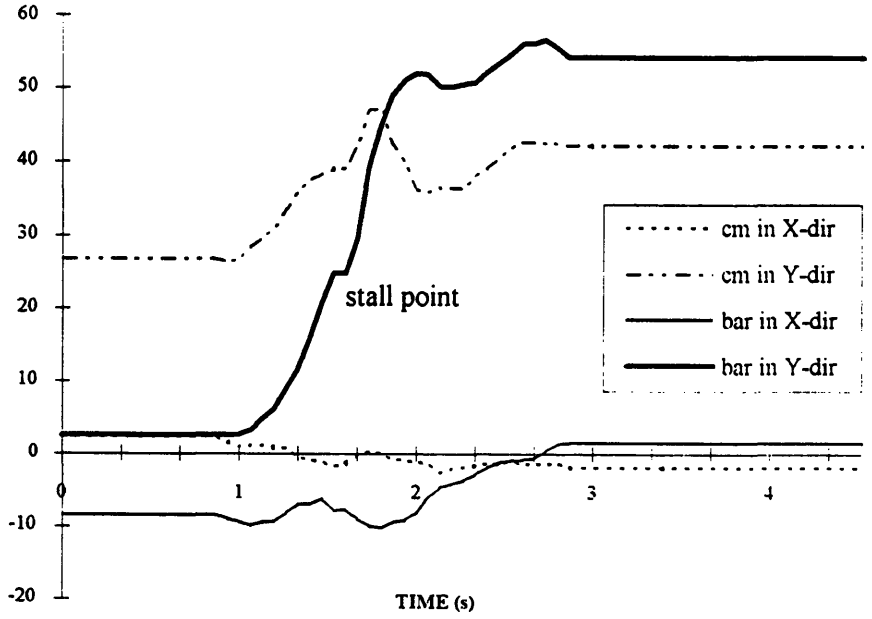

Figure 3.9: The vertical motion of the subject A's center of mass and bar

At the beginning of the lift, the force on the floor can be seen to start slightly before the force on the bar. The force on the floor then continues to increase and smoothly levels off, and the force on the bar abruptly peaks and then levels off (p1 in Figure 3.7). This detail shows the transfer of force to the mass through the subject's arms. The subject is able to transfer the large force produced by his legs through his arms since the subject's arms are in a singular configuration (see c2 in Figure 3.5). This configuration allows the structure of the subject's arms to bear the force. Once the mass is accelerated the force in the bar goes down compared to the force on the floor. The first dip d1 will be referred to as the stall point. This point is the instant when the weight reaches knee height, just before the large pull occurs. The stall point can also be seen in the trajectory of the bar in Figure 3.9. The body of the subject is now approaching a singular configuration and is capable of applying a very large thrust upwards. This thrust is clearly seen by the force produced on the floor by peak p2 shown in figure 3.7. During this peak (p2) the force on the bar increases slightly after the stall point (d1). Then there is a small dip (d2) which shows the transfer of force from the arms acting like ropes to the force (p3) created by the arms starting to pull on the mass as the body of the subject begins to leave the ground (shown in Figure 3.5 by configuration c3). During this part of the lift the body of the subject is now decelerating upward and begins to accelerate downward. The force on the floor (shown in Figure 3.7 by dip d4) becomes negative since we have subtracted the lifters weight. It is during this part of the lift that the subject is removing the energy stored in the mass of his body and transferring it through his arms to lift the mass. This can be seen in the trajectory graph (Figure 3.9) of the subject's body moving up and then down while the trajectory of the mass continues to move upward. This is similar to the door opening task strategy in which the body is first accelerated and then decelerated so that the bodies kinetic energy is transferred through the arm. After this motion in the lift, the subject is not capable of giving the mass any additional force since his arms are no longer near a singular configuration shown by configuration c4 in Figure 3.5. In this configuration during a quasi-static lift it would be necessary for the subject's arm muscles to bear the entire weight . At this time the subject comes abruptly back in contact with the ground.

This can be seen in the third very sharp peak force (p4) that occurs on the floor in figure 3.7. Since the mass is hanging instantaneously the subject positions himself at this time to accept the weight at his chest. The force peak on the bar that follows (p5) is the weight coming down on to the subject's chest and the oscillations that follow are caused by the vibration of the mass and the bar's compliance. The subject's arms are now able to bear the load since they are in another singular configuration. Once these oscillations stop the lifter can push upward using his legs. The lifter lifts, with the weight at his chest, from the crouched position to standing straight shown by position c5 in Figure 3.5. This simultaneous motion can be seen in the trajectory graph (Figure 9) between 2.25 sec and 3.0 sec. In Figure 3.7 there is a large dip (d5) that occurs simultaneously for both the force on the floor and the force on the bar. This dip is caused from the upward 'jump' after the push from the crouched position. The landing from this 'jump' can be seen as the next large peak (p6) followed by the oscillation of the subject and mass coming to rest.

Chapter 4
Dynamic Task Trajectories

A method for developing trajectories for a robot that satisfies the redundancy criterion will be presented in this chapter. Two dynamic tasks will be addressed; lifting dynamically and applying forces. The limitations of robots will be investigated to determine the most significant constraint in which to base a performance index. This performance index will be used to compute the capabilities and optimize trajectories for a dynamic robot.

4.1 Dynamic Robot Performance Index

4.1.1 Robot Performance Limitations

In the following section we will develop a performance index with which to evaluate the performance of our dynamic robot. We will define performance as a robot's ability to transmit power in terms of its weight. For example an increase in robot performance would mean an increase in transmitted mechanical power without increasing the robot's weight.

The aspects that limit a robots performance can be broken into three physical limitations: mechanical limits, control limits and electric motor limits. Mechanical limits define the limitations of the robots structure and internal transmission system (i.e. belts, gears, chains, etc.). Control limits are the limitations of the controller and the servo amplifiers. Electric motor limitations are the result of magnetic field saturation and the thermal limitation. These issues are constantly being addressed to increase the performance of today's robots. The most significant of all of the limiting factors is the thermal dissipation

limits of motors. Electric motors fail when the internal temperature rises to the break down temperature of the insulation. Our performance index will be based on the thermal break down of a motors insulation since this is the major limiting factor of robot performance.

4.1.2 Thermal Dissipation of Electric Motors

Heat dissipation, in general, is the limiting factor in motors. As energy is put into an electric motor some of the energy flows out as heat. If thermal energy flows in faster than thermal energy flows out of the motor the internal temperature will increase. If this temperature increases to the breakdown temperature of the wire insulation, the motor will fail.

A performance index can be developed by first examining the heat transfer of an electric motor. Permanent magnet brushed DC motors are considered here but a similar analysis can be extended to other types of motors. An electric motor can be modeled as an electrical resistance imbedded in a block of iron. For simplicity we will assume that the rotor has a uniform temperature distribution and thermal dissipation is due to convection. We will also assume radiation is insignificant. The flow of thermal energy can be represented by the following equation:

$$\dot{E}_g - \dot{E}_{out} = \dot{E}_{st}, \tag{4.1}$$

where $\dot{E}_g$ is the thermal energy generated by the electrical resistance of each motor, $\dot{E}_{out}$ is the thermal energy outflow due to convection, and $\dot{E}_{st}$ is the thermal energy stored in the mass of the rotor. The thermal energy generated can be written as

$$\dot{E}_g = I^2 R, \tag{4.2}$$

where I is the current that flows into the motor and R is the electrical resistance. The thermal energy flowing out of the motor can be modeled as convection:

$$\dot{E}_{out} = h\pi d(l + \tfrac{d}{2})(T - T_\infty), \tag{4.3}$$

where h is the convection heat transfer coefficient, $\pi d(l + \frac{d}{2})$ is the surface area of the rotor approximated by a cylinder, T is the temperature of the rotor and T_∞ is the room temperature. The energy stored in the mass of the motor can be written as

$$\dot{E}_{st} = c_p m_r \frac{dT}{dt}, \tag{4.4}$$

where c_p is the specific heat of the rotor and $m_r = \rho(\frac{\pi d^2}{4})l$ is the mass of the rotor.

A differential equation for the internal temperature of the rotor can be found by plugging equations (4.2), (4.3), (4.4) into equation (4.1):

$$\frac{dT}{dt} = \frac{I^2 R + h\pi d(l + \frac{d}{2})(T - T_\infty)}{c_p m_r}. \tag{4.5}$$

If we assume a constant flow of power into the motor equation (4.5), the solution can be written as

$$T = (\tfrac{I^2 R}{h(\pi dl)} + T_\infty)(1 - e^{-\frac{4h}{c_p \rho d} t}). \tag{4.6}$$

This equation can be used to find the internal temperature of the rotor as a function of time given some constant power input. Figure 4.1 shows the simulated internal temperature of a motor with a constant current input of 12 amperes.

In this simulation the motor has reached a steady state temperature after 600 seconds. This amount of time is much larger than any trajectory duration we will be examining.

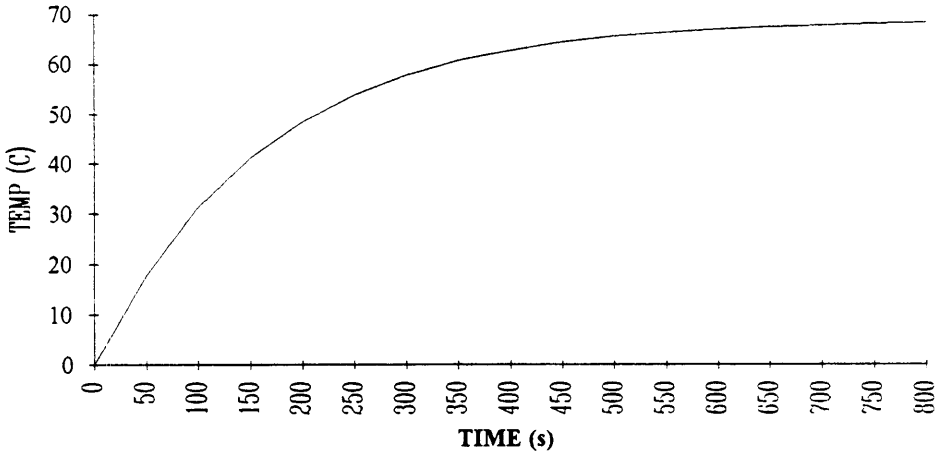

Figure 4.1: Computed temperature rise of motor.

Figure 4.2 shows the rise in temperature and the temperature decrease due to convection for the first 60 seconds.

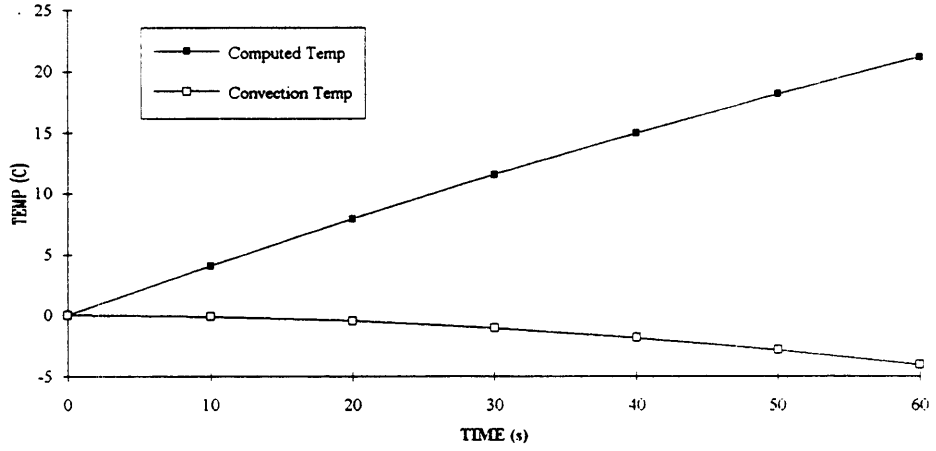

Figure 4.2: Computed temperature due to convection

It is apparent from this graph that for short durations the convection term is very small compared to the increase in temperature of the rotor.

All of the trajectories that we will be concerned with will be only a few seconds in duration. For these trajectories we can infer from the above simulation that the motor can

be modeled as an adiabatic system. This assumes that the thermal energy generated goes directly into heating the rotor and that the thermal energy dissipated from convection is negligible. We can write Equation 4.5 with this new assumption.

$$\frac{dT}{dt} = \frac{I^2 R}{c_p m_r}. \tag{4.7}$$

An experiment was performed to determine the validity of our model. A motor was instrumented with a thermistor positioned on its rotor, and the motor was supplied with an input of 12 amperes of current. The motor's output shaft was fixed so that the motor could not rotate. Temperature readings were recorded every ten seconds. A simulation was computed using Equation 4.7 with dimensions and other constants that were consistent to those used in the experiment. Figure 4.3 shows computed values compared with experimental data for a 50 second duration. The measured temperature was found to correlate well with the computed values from our adiabatic model.

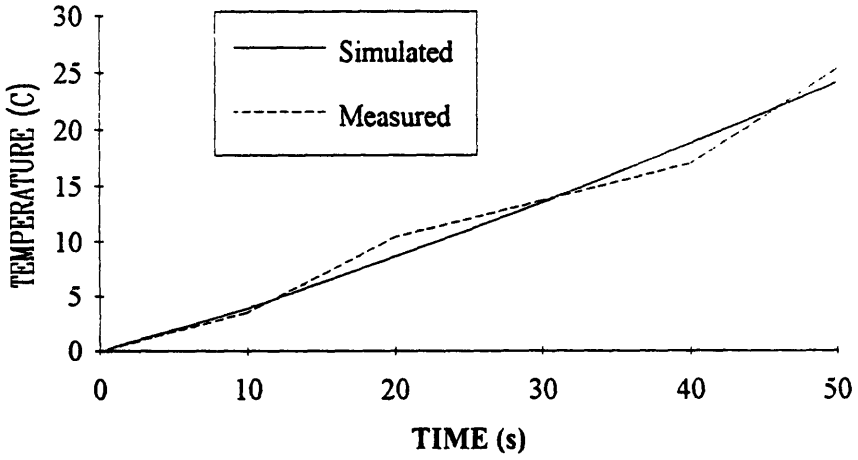

Figure 4.3: Experimental vs. computed

Equation 4.7 was computed for the case of constant power input, but for trajectory control of a robot the power input must be varied. We can rewrite equation 4.7 for a varying current input.

$$\frac{dT}{dt} = \frac{I(t)^2 R}{c_p m_r}, \tag{4.8}$$

where I(t) is the motor input current as a function of time. The input current as a function of time can be written in terms of the motor torque and motor torque constant.

$$I(t) = \frac{\tau(t)}{k_\tau} \tag{4.9}$$

We can find a differential equation for the temperature as a function of time and as a function of the torque trajectory for the motor by substituting Equation 4.9 into Equation 4.8.

$$\frac{dT}{dt} = \frac{\tau(t)^2 \frac{R}{k_\tau^2}}{c_p m_r} \tag{4.10}$$

This equation can be solved numerically using torque trajectory inputs to compute the temperature rise of the motor's rotor.

Figure 4.4. and 4.5 are an example torque trajectory and resulting temperature rise respectively.

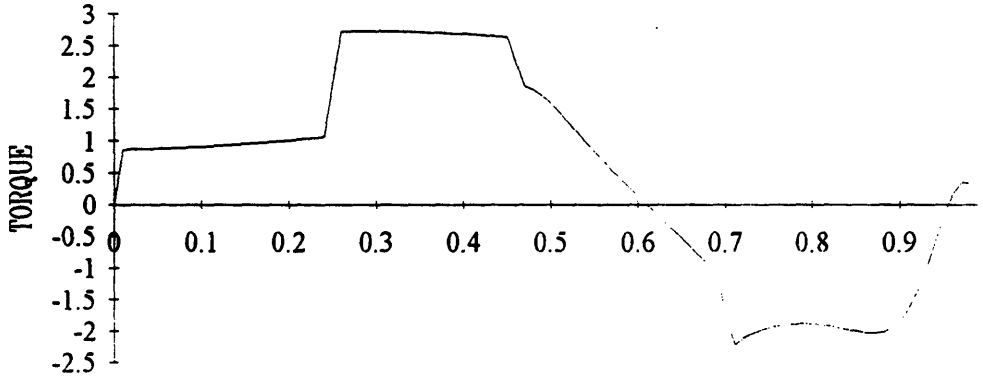

Figure 4.4: Torque trajectory

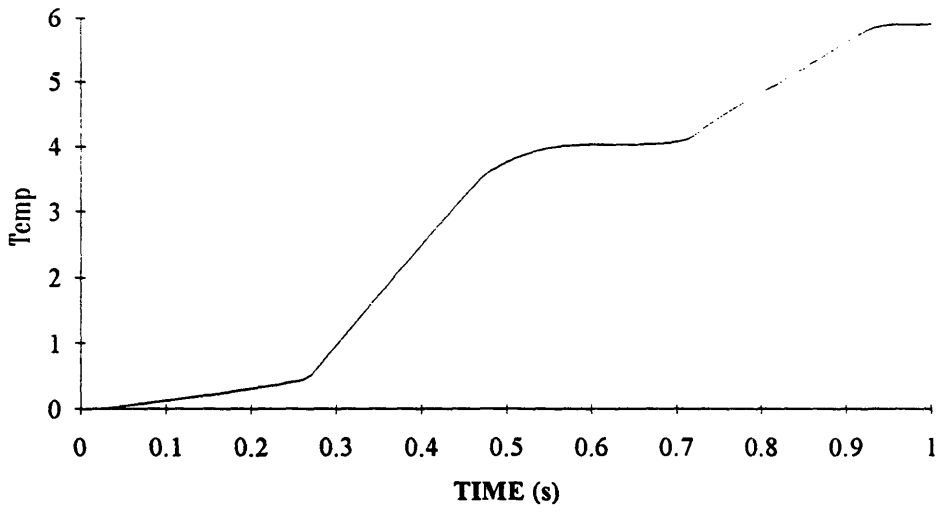

Figure 4.5: Computed temperature

From this analysis we find that the performance index should be based on the integral of torque squared over the duration of the trajectory.

4.2 TRAJECTORY SYNTHESIS

4.2.1 Outline of the Synthesis Method

In this section, an optimal trajectory for the four degree-of-freedom dynamic robot to produce forces and lift objects will be generated based on the motion data acquired from human motion. It should be noted that the trajectories of humans are not directly applicable to the robot, because the human and the robot are not identical in kinematic structure, mass distribution, and actuators. Although we intend to design the robot so as to perform dynamic tasks in a similar way, the robot has fewer degrees of freedom, in addition to the physical differences. Therefore, instead of copying the original human data, we need to extract features essential to the dynamic motion strategy and apply them to the robot. Specifically, our method for synthesizing an optimal trajectory is summarized by the following steps:

1) Extract a motion pattern from human data, and parameterize the motion with a set of variables in such a way that the parameterized motion pattern can elucidate the human dynamic motion strategy,

2) formulate an optimization problem with respect to the trajectory parameters by using the robot's dynamic equations and a performance index for evaluating the robots task performance and

3) solve the optimization problem using a recursive optimization algorithm with initial values obtained from the human data.

To fill the gap between the human and the robot as well as to generate a trajectory optimal for the robot rather than the human, we formally describe an optimization problem using a performance index defined specifically for the robot. Solving such an optimization problem, however, is a difficult task due to non linearity and local minima. To overcome the difficulties, we again use the human data for the purpose of providing a set of appropriate initial values. Since the robot and the human are topologically similar in their construction, it is initially assumed that an optimal robot trajectory can be obtained in a region near the human data. This allows us to reduce a global optimization problem to a certain local optimization and avoid local minima and difficult non linearity problems.

Extracting a motion pattern from the human data allows us to parameterize a motion to be used for the purposes of optimizing the trajectories for the robot. These parameterized trajectories are derived from the human measured trajectories. The trajectories should be parameterized with a sufficient number of parameters that describe the dynamic task. The forces produced from the dynamic motion of the centroid can be computed by subtracting the forces measured at the end effector from the forces measured at the base. The information found from this calculation indicates the relevant elements of the motion trajectories responsible for producing the dynamic forces. This information guides us in selecting the minimum number of parameters that describes the motion, which describes

the gross motions of the center of mass and end effector in the regions where the forces are produced dynamically.

The trajectories are based on a string of sequences of constant acceleration acting for a interval of time. Constant accelerations were chosen since the human trajectories were observed to be made up of a series of constant acceleration sequences. The parameters chosen to describe the trajectories consist of a number of constant accelerations A_i that act for a duration of time t_i for each sequence. A minimal number of sequences capable of describing the forces produced during the dynamic task. The initial and final conditions on these trajectories can be defined by the task or also used as parameters. The parameterized trajectories of the center of mass and end effector can be written

$$R(t) = \tfrac{1}{2} A_i (t - t_{i-1})^2 + V_{i-1}(t - t_{i-1}) + R_{i-1} \tag{4.11}$$

$$r(t) = \tfrac{1}{2} a_i (t - t_{i-1})^2 + v_{i-1}(t - t_{i-1}) + r_{i-1} \tag{4.12}$$

$$\text{for } t \in [t_{i-1}, t_i] \quad i = 1, \ldots, s$$

where

$$R_{i-1} = R(t_{i-1}), \qquad r_{i-1} = r(t_{i-1}) \tag{4.13}$$

$$_{i-1} = \frac{dY}{dt}\Big|_{t=t_{i-1}}, \qquad v_{i-1} = \frac{dy}{dt}\Big|_{t=t_{i-1}}$$

where $R(t)$ is the parameterized trajectory of the center of mass, $r(t)$ is the parameterized trajectory of the robot end effector, s the number of sequences and R_{i-1}, r_{i-1}, $_{i-1}$, and v_{i-1} are the boundaries for each time sequence.

Figure 4.6 shows a block diagram of the optimization technique. Initial values for the parameters can be found from the human data. Boundary conditions and trajectory parameters can be established based on the desired result from the dynamic task.

Let **b** be the vector consisting of the boundary conditions of the trajectory. Let **p** be the vector consisting of the parametric representation of the trajectories:

$$\mathbf{b} = [R_0, R_f, r_0, r_f, V_0, V_f, v_0, v_f] \tag{4.14}$$

$$\mathbf{p} = [A_1, \ldots, A_s, a_1, \ldots, a_s, t_1, \ldots, t_s]. \tag{4.15}$$

Let **q** be the vector that combines the parameters and boundary conditions

$$\mathbf{q} = [\mathbf{b}, \mathbf{p}]^T. \tag{4.16}$$

The final parameters that are to be optimized should be completely independent so that the number of parameters are minimized. By setting boundary conditions on the trajectories many of the parameters become dependent. Equations (4.11) (4.12) and (4.13) that describe the position trajectory of the end effector and centroid are written in terms of the constant accelerations, time intervals, and boundary conditions. These equations can be used to find the relationship of the terms in **q** (equation 4.16) to find an independent set of parameters.

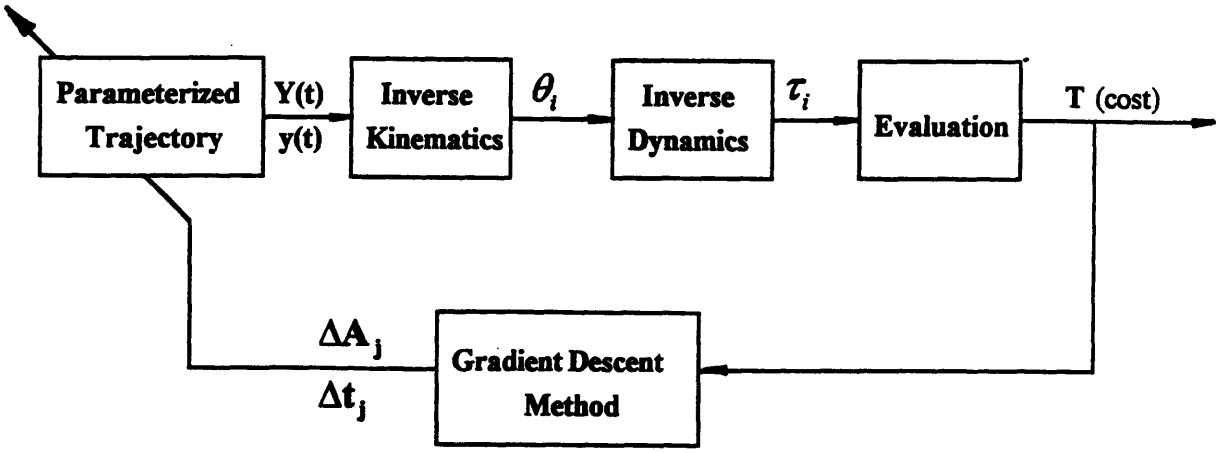

Figure 4.6 The optimization process

For each iteration of the optimization the position equations are used to find the motion trajectories. Using a kinematic model of the robot the inverse kinematics can be computed. In the case of a redundant robot the inverse kinematics can be computed by adding the constraint of the center of mass trajectory. This method is describe in section 2.7. This computation will provide joint angle trajectories for our robot. We assume these trajectories can be differentiated (closed form or numerically) to find the angular

velocities and angular accelerations of the joint angles. Actuator torques necessary to move the end effector and center of mass through the motion trajectories can be computed using the equations of motions for the robot model. The Lagrange equations of motion of a robot can be written in terms of the joint positions, angular velocities, and angular accelerations [Asada and Slotine, 1986]

$$\tau_i = \sum_{j=1}^{n} H_{ij}\ddot{\theta}_j + \sum_{j=1}^{n}\sum_{k=1}^{n} h_{ijk}\dot{\theta}_j\dot{\theta}_k + G_i \qquad i = 1,...,n \tag{4.17}$$

where coefficients H_{ij}, h_{ijk}, and G_i are functions of joint displacements $\theta_1,...,\theta_n$.

Using a performance index the motion and torques can be evaluated. This performance index should be based on a quantity that is desired from the dynamic task. The performance index can be based on any of the terms computed for our robot model. The performance index can be written in a general form

$$PI = f(\tau(t)_i, \theta(t)_i, \dot{\theta}(t)_i, \ddot{\theta}(t)_i) \qquad i = 1,...,n \tag{4.18}$$

where n is the total number of degrees of freedom and therefore the number of actuators. For the case studies presented in this thesis the performance index is based on the integral of the torque squared (heat of the motors) and the goal of the optimization is to minimize the final temperature of the hottest motor.

An optimization technique is needed in which to optimize our parameterized trajectories in terms of our performance index. Because of the highly nonlinear properties of the optimizations numeric methods should be used. For our case studies the gradient decent method was selected. Assuming that the initial conditions were chosen appropriately the program should converge to a optimum. We assume that an optimal robot trajectory can be obtained in a region near the human data since the robot can move

in a similar fashion to the human performing the task. After a number of iterations the final trajectories can be found once the performance is sufficient. It is expected that an optimal solution will be found within a region in the parameter space that includes the general form of the human motion.

4.2.2 Parameterization of Human Lifting Trajectories

In this section we will parameterize trajectories for the task of dynamic lifting. Based on the physical interpretation of the athlete's lifting data addressed in Section 3.4.3, we will extract a motion pattern, or a template for the purpose of the robot trajectory optimization. Essential to the human dynamic lifting is that the body centroid motion is precisely coordinated with the motion of the arms that hold a barbell. Therefore, we must generate two trajectories for coordinated movements. Also manifested in the human data is that the lifting process comprises several distinct stages in which both the body and the barbell exhibit discrete changes in their motions, as described in Section 3.4.3. Based on these observations, we will generate a motion pattern described by a pair of trajectories consisting of several segments. We will focus our attention to the dynamic part of the trajectory and omit the final push upward.

Figure 4.7 shows trajectory patterns for the body and the barbell motion divided into n segments, called intervals. Note that compared with the large motions in the vertical direction, i.e. the y-axis, the horizontal motions are insignificant, hence ignored in the figure. In each interval of the segmented trajectories, the acceleration of the body centroid as well as the acceleration of the barbell are assumed to be constant. Let A_i and a_i be, respectively, the acceleration of the body centroid and the acceleration of the weight during the i-th interval, $t_{i-1} \le t < t_i$.

The position trajectories of the body centroid and the weight, denoted Y(t) and y(t), respectively, are given by

$$Y(t) = \tfrac{1}{2} A_i (t - t_{i-1})^2 + V_{i-1}(t - t_{i-1}) + Y_{i-1} \tag{4.19}$$

$$y(t) = \tfrac{1}{2} a_i (t - t_{i-1})^2 + v_{i-1}(t - t_{i-1}) + y_{i-1} \tag{4.20}$$

$$\text{for } t \in [t_{i-1}, t_i], \ i = 1, \ldots, n$$

where

$$Y_{i-1} = Y(t_{i-1}), \qquad y_{i-1} = y(t_{i-1}) \tag{4.21}$$

$$V_{i-1} = \frac{dY}{dt}\Big|_{t=t_{i-1}}, \qquad v_{i-1} = \frac{dy}{dt}\Big|_{t=t_{i-1}}.$$

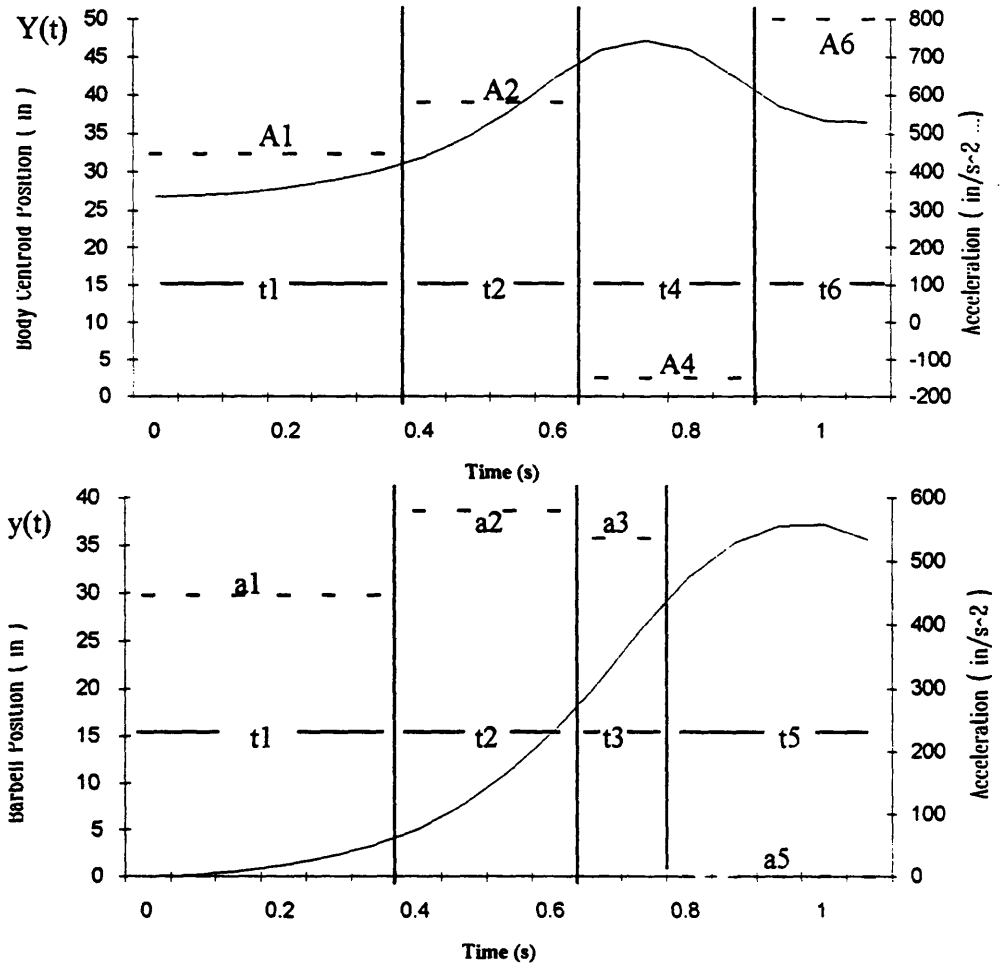

Figure 4.7: Trajectories derived from human weight lifting motion

The number of segments, n, is determined based on the physical interpretation of the human lifting data. As discussed in Section 3.3, the human lifting strategy is interpreted in

the five distinct stages shown in Figure 3.5: c1) the squat, c2) the initial leg extension, c3) the up and down motion, c4) the catch, and c5) the vertical push.

During each stage, the measured human data can be approximated as a constant acceleration motion except for some points on the trajectories. For example, the measured data show a stall point, which correspond to the rotation of the back for balancing the whole body in the x-direction. Our robot does not have this degree of freedom, but is capable of effectively lifting an object. We removed these details involved in the human data and compared the data with the segmented trajectory model. Figure 4.8 shows a comparison of the model with the human data. The individual accelerations A_i and a_i, and the time intervals t_1 through t_6, are determined by using a standard curve fitting technique: the minimum squared error criterion. As shown in the figure, the model

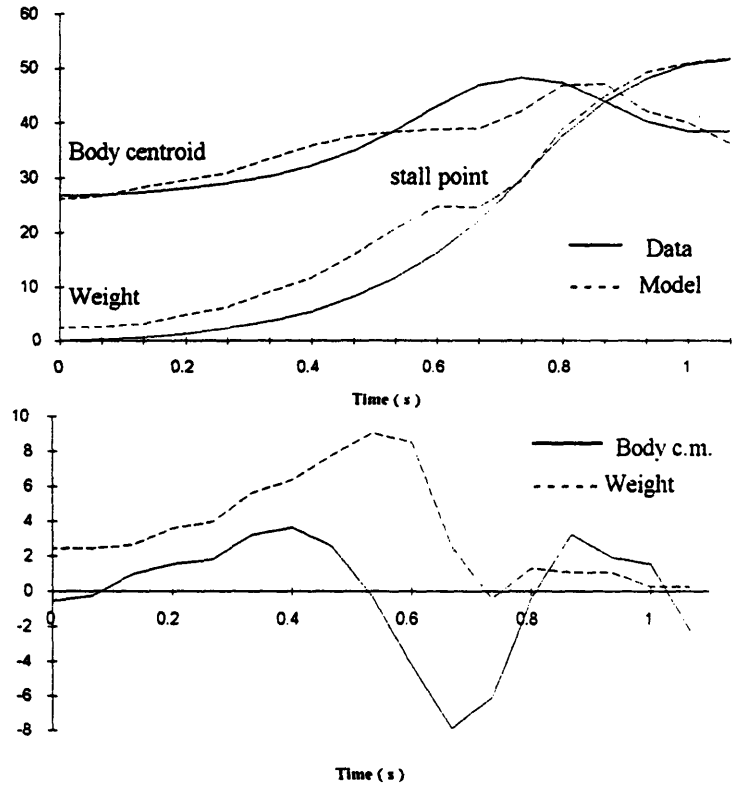

Figure 4.8: Comparison of human trajectories to derived trajectories

trajectory would be almost the same as the human data everywhere except for the presence of the stall point. Therefore the simplification of the trajectories using constant accelerations in the five distinct segments is valid for modeling the human motion. In generating optimal trajectories for the robot, we will use these accelerations and time intervals as the parameters to characterize the trajectories.

4.2.3 Parameterization of Applying Force Trajectory

In this section we will extract a motion pattern for the task of creating dynamic forces to a fixed point in the robots work space. An example of this type of force creation is the door opening task described earlier. This task uses a simpler trajectory than for the task of lifting. For this task the robot's base and end effector will remain fixed in space and only the body centroid of the robot is manipulated on a trajectory that results in a force being produced at the end effector. Therefore, there is only a need to generate a single trajectory. From the measured human data of the door opening task, we find that there are three distinct stages, as described in Section 3.2.3.

Figure 4.9 shows trajectory patterns for the body motion divided into the three intervals. In each interval of the segmented trajectory, the acceleration of the body centroid are assumed to be constant. As in the case of lifting we will let A_i be the acceleration of the body centroid during the i-th interval, $t_{i-1} \le t < t_i$.

The position trajectory of the body centroid, denoted X(t) is given by

$$X(t) = \tfrac{1}{2} A_i (t - t_{i-1})^2 + V_{i-1}(t - t_{i-1}) + X_{i-1} \qquad (4.22)$$

$$\text{for } t \in [t_{i-1}, t_i] \quad i = 1, \ldots, n$$

where

$$X_{i-1} = X(t_{i-1}) \quad {}_{i-1} = \frac{dX}{dt}\Big|_{t=t_{i-1}} \qquad (4.23)$$

After studying the human task of opening a stuck door we can determine the number of intervals during the task of dynamically producing forces. The first interval is when the center of mass is accelerated by a force generated by the humans legs. The next interval begins when the applied force is generated by the deceleration of the center of mass through the arm in the vicinity of a singular configuration. The applied force is then followed by the final interval, where the recovery force decelerates the centroid back to rest. Fig. 4.9 shows a idealized graph of the motion of the center of mass. This graph assumes that the forces acting are constant during each phase. The initial acceleration is

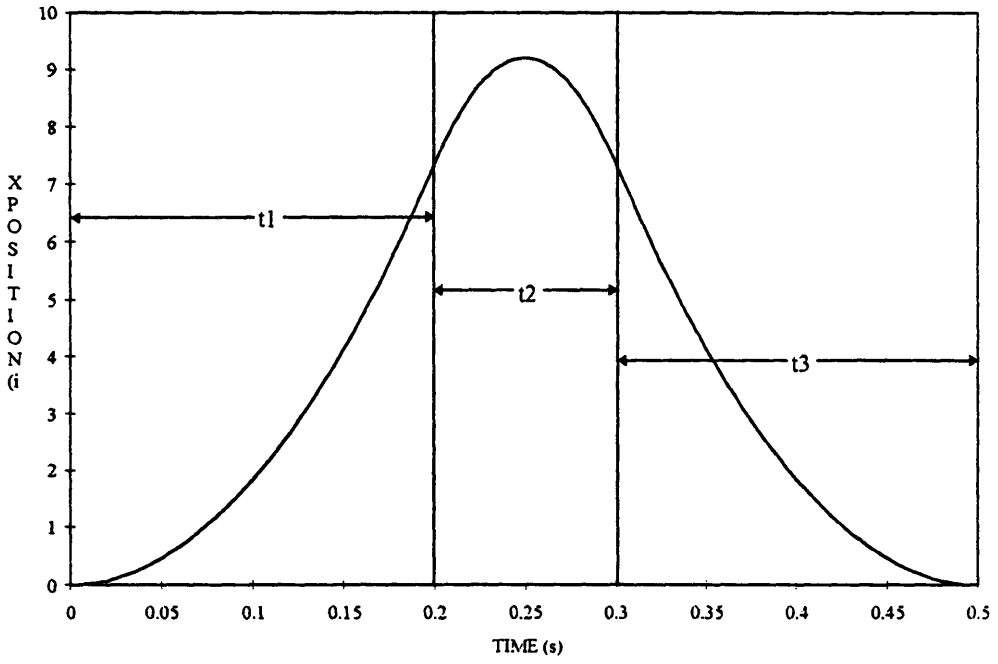

Figure 4.9: Trajectory derived from human motion

due to the initial force. The large deceleration results in the production of the applied force and the final acceleration is due to the recovery force.

The goal is to find trajectories for the task of lifting objects and applying forces that optimize our performance index. In the following section we will develop an optimization

technique that can be used to compute feasible trajectories for our robot to perform each of these dynamic tasks..

4.2.4 Formulation of the Optimization Problem

For the robot described in Section 2.8, optimal trajectories will be obtained by using the parameterized models described above for the task of lifting objects and producing forces dynamically. To this end, we first define a performance index based on Equation 4.10 to evaluate the motion trajectories. The aim of human dynamic motion is to maximize the force exerted with a limited muscle power. Namely, the strategy is to best alleviate the worst case, or minimize the hottest actuator. In this paper, we consider the performance index

given by

$$PI = \underset{1 \le j \le n}{Max} \int_0^{t_f} (\tau_j(t))^2 dt, \tag{4.24}$$

where $\tau_j(t)$ is the torque of the j-th actuator, n is the number of actuators and t_f is the final time of the motion.

Exerting large torques for a long time incurs a fatigue in muscles as well as an overheat problem in electric motors. In this sense the dynamic strategy is particularly effective with respect to fatigue and power consumption, because, as we observed, the dynamic motion requires large torques only for a limited period of time, hence no fatigue and no overheating. This is critically important for electric motors and makes a significant difference in performance, because the instantaneous rated torque of a motor is much larger than the continuous rated torque. As long as the duty cycle is low, electrically powered robots can exert large forces. Since it is unlikely to produce large forces very often or at high duty cycles, the dynamic robot described in the previous section produces much larger forces dynamically and quicker than that of slow, quasi-static forces. To this end, we have selected a special type of motors for the dynamic robot: the motors have large instantaneous rating torques compared with continuous torques. In so far as the

dynamic motion is completed in a short period of time, the duty cycle requirement is satisfied. Therefore we impose the following condition on the optimization problem

$$t_f \leq T_f, \tag{4.25}$$

where T_f is the maximum allowable period of dynamic motion.

The performance index, Equation. (4.24), varies depending on the parameters of the trajectories. For the case of lifting it depends on the parameters for both the body centroid and the barbell trajectories and for the case of applying forces only the centroid trajectory is of interest. From Equation 4.15 **p** is the vector consisting of all the parametric representation of the trajectories.

$$\mathbf{p} = [A_1,\ldots,A_n,a_1,\ldots,a_n,t_1,\ldots,t_n]^T \tag{4.26}$$

The above parameters, though, are not totally independent because of the boundary conditions that the trajectories must satisfy. For the task of lifting, the weight must be moved from the floor to a designated height, and for the task of applying a force, the end effector must remain fixed. For both cases the end effector and the centroid start at a zero velocity and finishing at a zero velocity as well, i.e. a rest-to-rest trajectory. Therefore the end effector has the following constraints:

$$\begin{aligned} y_0 &= y(0), & v_0 &= \frac{dy}{dt}\Big|_{t=0} = 0. \\ y_n &= y(t_n), & v_n &= \frac{dy}{dt}\Big|_{t=t_n} = 0. \end{aligned} \tag{4.27}$$

Similarly for the body centroid trajectory:

$$Y_0 = Y(0)_i, \qquad \mathbf{V}_0 = \frac{dY}{dt}\Big|_{t=0} = 0. \tag{4.28}$$

$$Y_n = Y(t_n), \qquad \mathbf{V}_n = \frac{dY}{dt}\Big|_{t=t_n} = 0.$$

where y_f is the final designated height of the weight. The performance index is then a function of the parameters **p** and the boundary conditions **b**; $\mathbf{q} = [\mathbf{b}, \mathbf{p}]^T$ and PI=PI(**q**). Therefore the trajectory optimization problem is formally stated as:

$$\text{Minimize } PI(\mathbf{q}) = \max_{1 \le j \le n} \int_0^{t_f} (\tau_j(t))^2 dt \tag{4.29}$$

subject to

i) the robot dynamic equations, (4.17)

ii) the parametric trajectory representations, (4.11),(4.12),(4.13),

iii) the boundary conditions, (4.27), (4.28), and

iv) the total time condition, (4.25).

Note that the boundary conditions can be solved explicitly by using the parametric trajectory representations, which are all kinematic and algebraic relationships. Therefore, we can reduce the parameter vector **q** to a compact one with all independent variables. We will use this independent set of variables for the optimization in the following section.

4.3 Optimal Trajectories

4.3.1 Optimization

Since the optimization problem formulated in the previous section is highly nonlinear, only numerical methods are applicable. We use a gradient descent method for solving the problem. Note, however, that the performance index function P(**q**) is not completely differentiable due to the Max-function involved. As a result, the gradient direction varies discretely in the vicinity of the rough terrain of the performance function. To alleviate an unwanted zigzag motion in the optimization process, a momentum term is added to the gradient.

Namely,

$$\mathbf{q}[k+1] = q[k] + \Delta\mathbf{q}[k] \tag{4.30}$$

$$\Delta\mathbf{q}[k] = -\alpha\nabla P + \beta\Delta\mathbf{q}[k-1]$$

where ∇P is the gradient of the performance index, α and β are coefficients, and the second term, $\beta\Delta\mathbf{q}[k-1]$, is the momentum term for smoothing out the gradient direction.

To compute an optimal solution, an initial estimate of parameter vector **q** must be provided. As mentioned previously, we use the human data to provide initial values for the recursive optimization. It is expected that an optimal solution will be found within a region in the parameter space that includes the experimental data point. This not only alleviates the difficulty in solving a global optimization problem, but also allows for generating effective trajectories similar to the human motion.

4.3.2 Lifting Trajectory Results and Discussion

Figure 4.10 shows the initial trajectories derived from the motion of the lifted mass and centroid of the subject, as well as the final trajectories that have been optimized for our dynamic robot by varying the trajectory parameters to minimize the maximum temperature by the calculations described in the previous sections. The optimum trajectory was reached after about 75 iterations.

A comparison trajectory was synthesized to compare to the optimized trajectory. This trajectory was chosen to show the benefits of the dynamic lifting technique. The comparison trajectory was synthesized with the same boundary conditions on position and velocity (Eqs. 4.27 and 4.28) and for the same length of time as the optimized trajectory. The trajectory was designed with a constant acceleration for the lifted mass and another constant acceleration for the robots centroid to be active for half of the total time and displacing half of the total displacement and then decelerating with the same magnitude

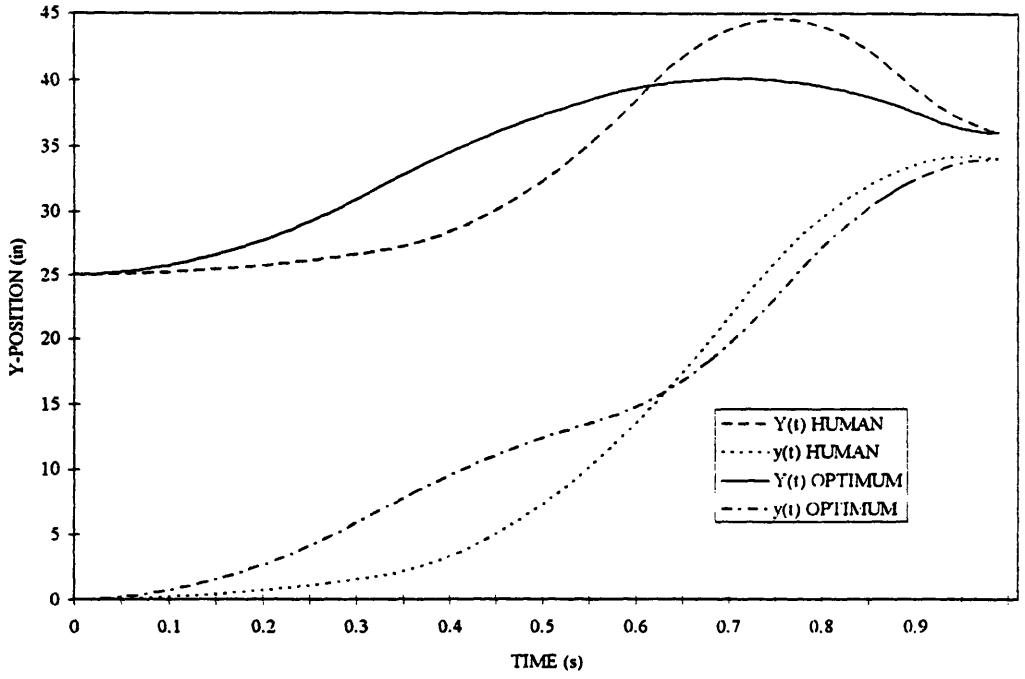

Figure 4.10: The initial and optimized trajectories

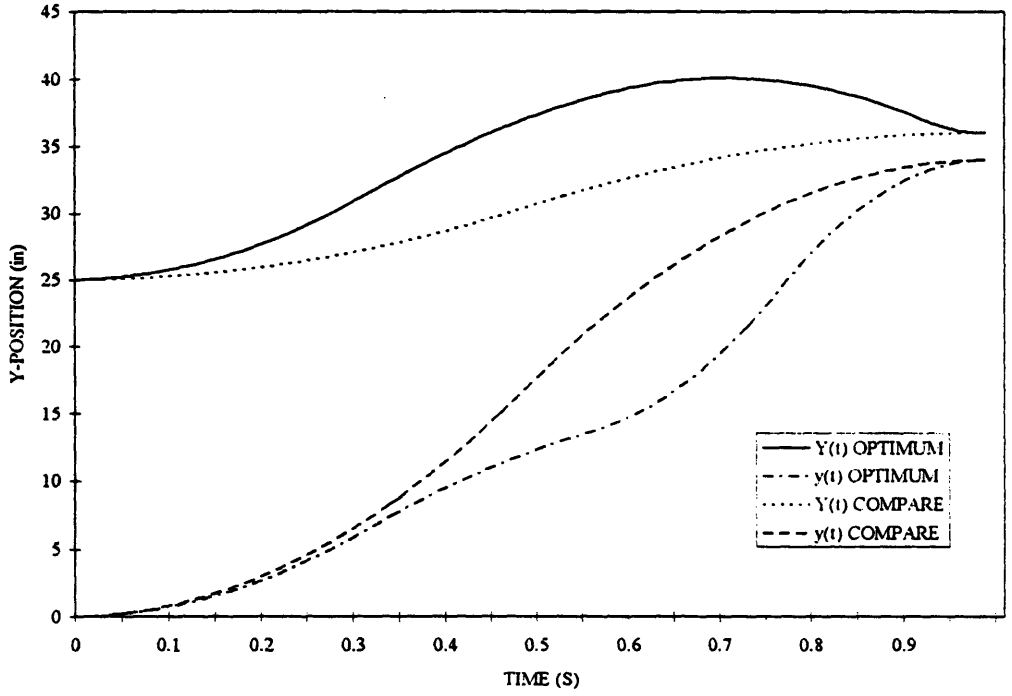

Figure 4.11: The optimal and comparison trajectory

accelerations for the remaining half of the trajectory. This is a common high speed trajectory technique. These trajectories are compared to the optimal lifting trajectories, shown in Figure 4.11.

The torque trajectories were computed using the equations of motion derived in Section 4.2. Figure 4.12 shows the computed torque trajectories of motors 1 and 2 for the optimized and comparison trajectories shown in Figure 4.11. Note that the torque for motor 2 is larger in places and more constant for the comparison trajectory than the torque needed for the optimized trajectory.

Figure 4.13 shows the torque trajectories computed for motors 3 and 4 for the optimized and comparison trajectories. Note that in the optimum case the maximum torque for both of these motors was larger than in the comparison trajectory, although for most of the time the torque needed for the comparison trajectory are larger.

Figure 4.10 shows the transformation of the initial human inspired trajectories to the computed optimum trajectory. Although the peak has been decreased and the trajectory is smoothed the optimum trajectory contains the same features as those observed in the human motion. Using the mechanical advantage ellipsoids presented in Section 2.9, we can examine three instances during the trajectory. Figure 4.14 shows the ellipses superimposed onto the centroid and end-effector for three configurations. The ellipse represents the ability for the robot's arm and leg to create a force in any direction given an equal power distributed among the actuators. In the first configuration the ellipse's major axis is in the vertical direction showing a favorable configuration of the arm to create a large pull upward on the mass in the initial stages of the lift. The second configuration shows a unfavorable configuration for the arm to be pulling on the mass. The trajectory is such that the mass is pulled rapidly through this weak configuration (acting almost as a projectile). In the third configuration the mass has been completely lifted and the ellipse is very large in the vertical direction showing the ability for the robot to easily hold the mass in this configuration.

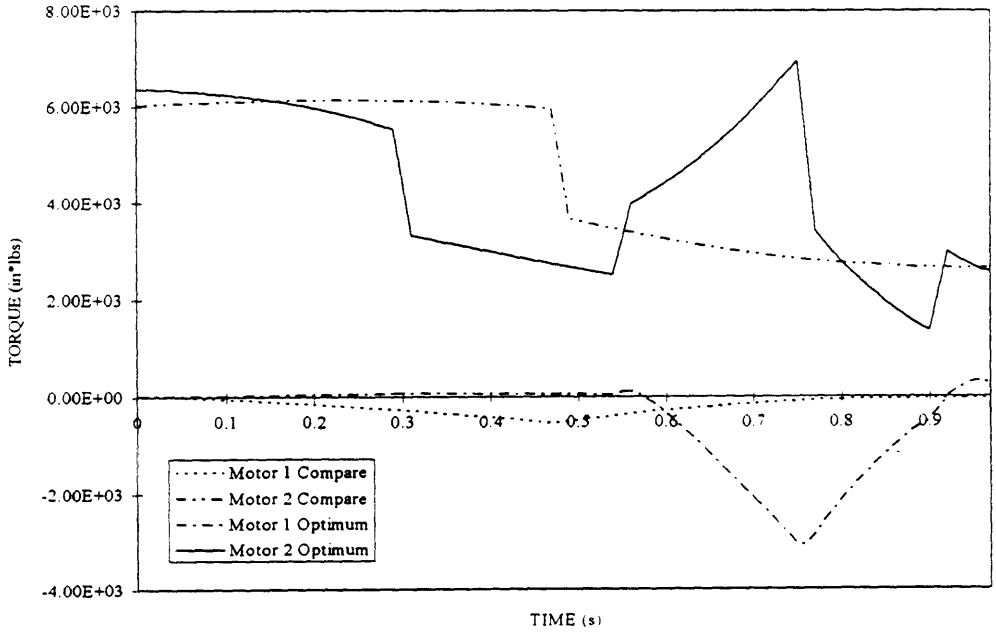

Figure 4.12: Torque trajectory comparison for motor 1 and 2

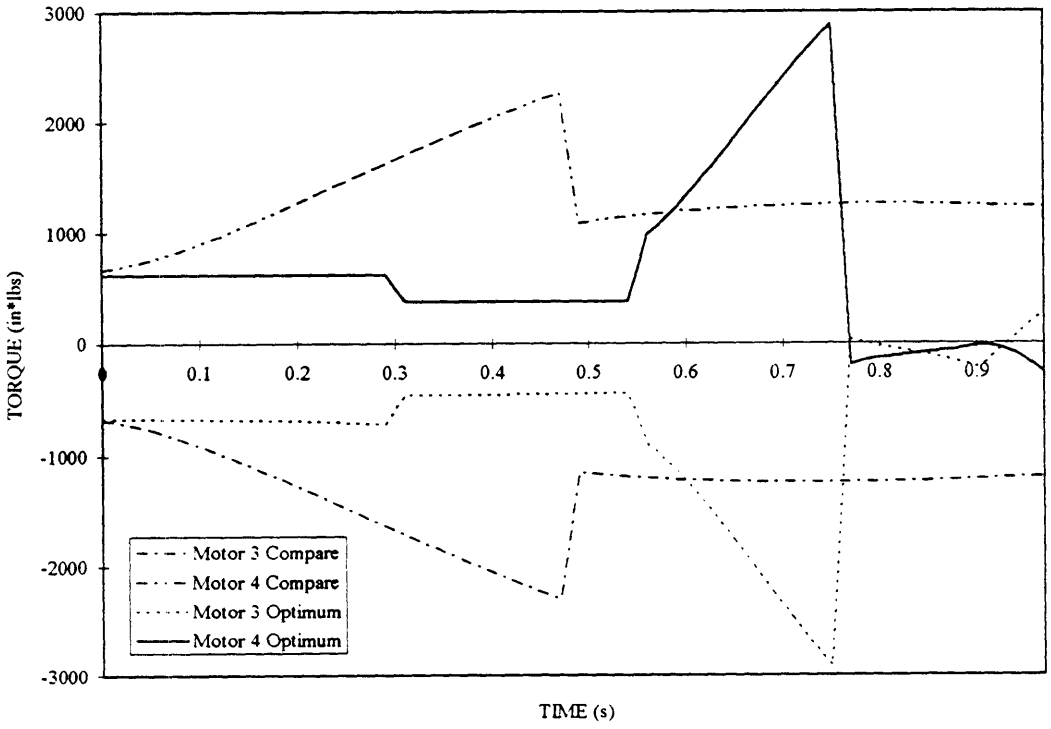

Figure 4.13: Torque trajectory comparison for motor 3 and 4

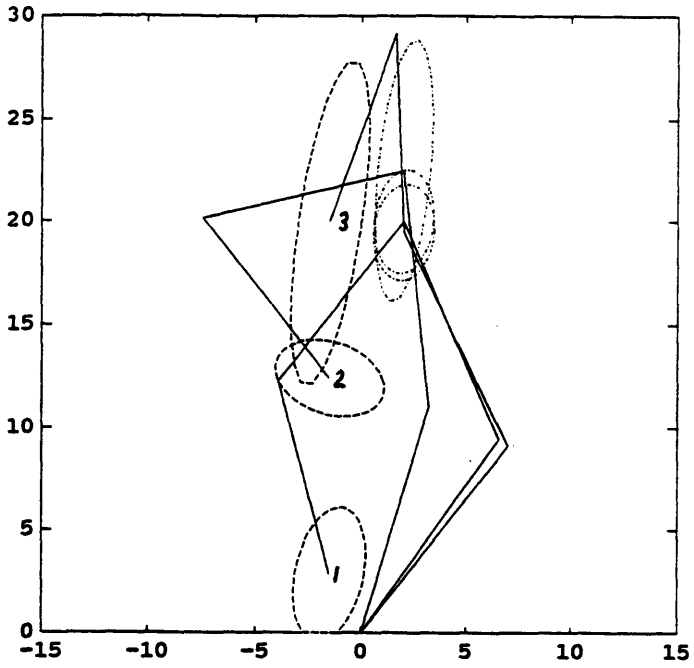

Figure 4.14. Mechanical Advantage superimposed on configurations for dynamic lift

The torques shown in figure 4.12 and 4.13 show that, for most of the time the actuators, for the optimum trajectory required less torque than the comparison trajectory. The computed torque for the optimum case required the actuators output to fluctuate much more than the comparison trajectory. This fluctuations take advantage of the fact that electric actuators have much greater peak outputs than continuos output. The performance index, which computes the temperature of the hottest motor, was found to reach a higher temperature for the comparison trajectory. This fact shows that using a dynamic technique would allow a robot to lift a greater weight in the same amount of time.

The temperature increase that each motor would occur can be computed using,

$$\Delta T_{m_i} = C_i \int_0^{t_f} \tau_i(t)^2 dt \qquad i = 1,\ldots,4 \qquad (4.31)$$

where C_i is the thermal constant of each motor and $\tau_i(t)^2$ is the torque trajectory of each motor. Figure 4.15 shows the temperature comparison for each motor.

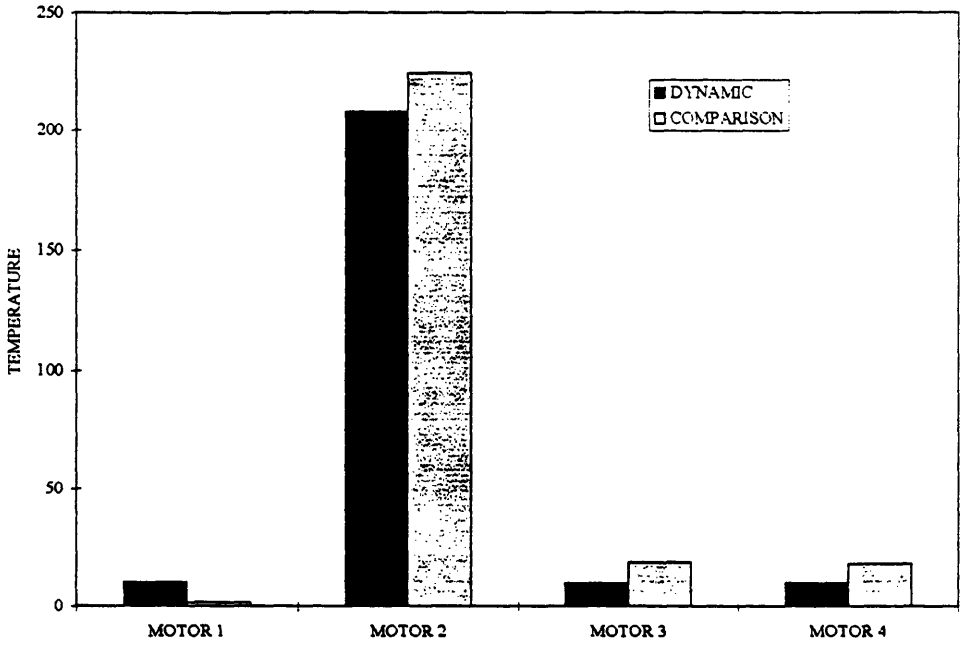

Fig 4.15. Temperature rise comparison for lift

Motors 2, 3, and 4 heat up less using the dynamic method while Motor 1 heats up more. Note that Motor 2 heats up significantly more than the other Motors for both methods. It is apparent that the optimization used Motor 2's temperature as the cost function.

By summing the temperatures of all the motor for each method we can compute a value that is proportional to the energy dissipated. The dynamic method for this case was found to use 7% less dissipated energy than the comparison trajectory.

4.3.3 Optimization for the Case of Applying Forces

For the task of applying forces the actuator torque for each instant in time can not be computed from the trajectory of the centroid alone. Since the base and end effector of our multi-degree of freedom robot is fixed to ground, the robot is left with n actuators and n-2 degrees of freedom. This would imply that there was an infinite number of combinations of actuator torques that could move the robots centroid through a given trajectory. For

the optimization we will not include the force component due to gravity. Gravitational forces will be added in after optimizing and will be assumed to be borne by the bottom links. We can write the relationship of the necessary force to accelerate the centroid through the parameterized trajectory in terms of the actuator torques. This can be written as:

$$\mathbf{F}_m = \mathbf{J}_m^T \mathbf{Q}_R \tag{4.32}$$

where the relationship can be written using the Jacobean transpose. By taking the pseudo-inverse of this Jacobean relationship we can find a least squares optimum for the instantaneous torques needed. The next problem is to find the optimum trajectory over time that minimizes the performance index.

A similar optimization technique that was applied to the case of lifting objects will be used for the case of applying forces. In this case we are specifying an amount of force that we would like to apply by the end-effector fixed to the environment. We will constrain the problem by also specifying t_2 the duration of the this force. Another constraint we can place on the optimization problem is that the trajectory is symmetric. This assumes that the initial acceleration to the centroid during the first stage and the final deceleration during the third stage is equal and produced for equal durations. This symmetry can also be seen in the human trajectories. For this optimization the total time of the trajectory will be added as a parameter to vary. The optimization technique used for computing optimal lifting trajectories can be apply to this task. An optimal solution that minimizes our performance index (Equation 4. 29) can be computed.

4.3.4 Results and Discussion of Applying Force Task

Figure 4.16 shows the final optimal trajectory for the task of applying forces. This optimum was reach after 23 iterations. For the task of producing a 65 lbs force for a period of .20 seconds a optimum total length of time for the trajectory was found to be 1.23 seconds.

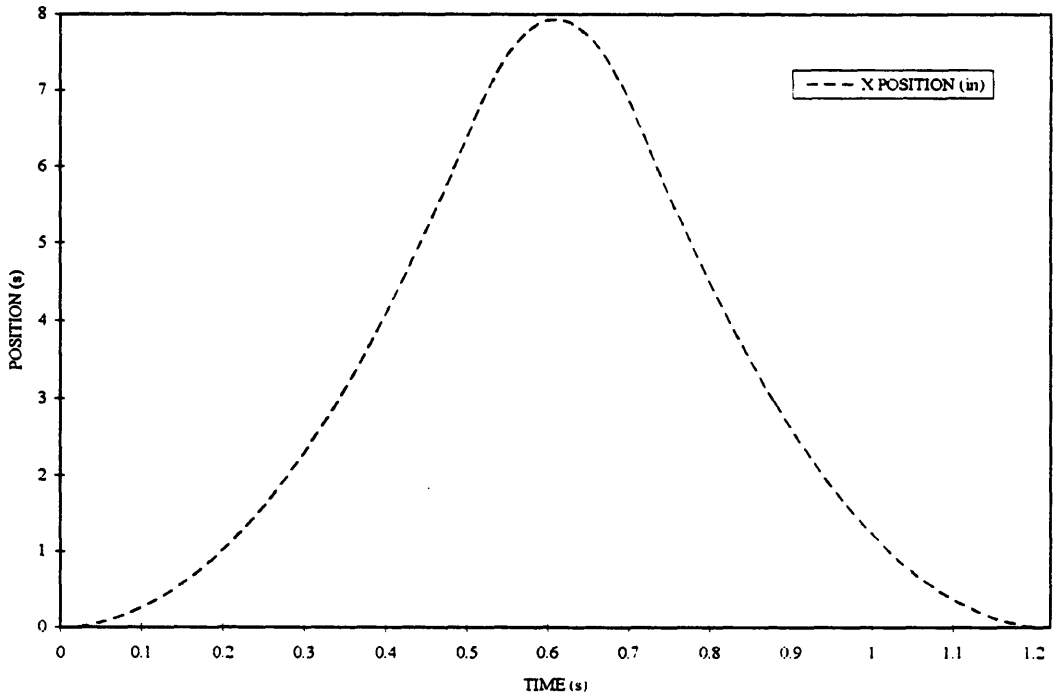

Figure 4.16: The optimal trajectory for producing a force

The torques were computed using from the optimal trajectory shown in Figure 4.16. The resulting torques for all four motors are shown in Figure 4.17. Notice that the torque of motor 1 and 2 are much larger than motor 3 and 4. The torque necessary at the beginning and end of the middle time sequence requires large peak torques.

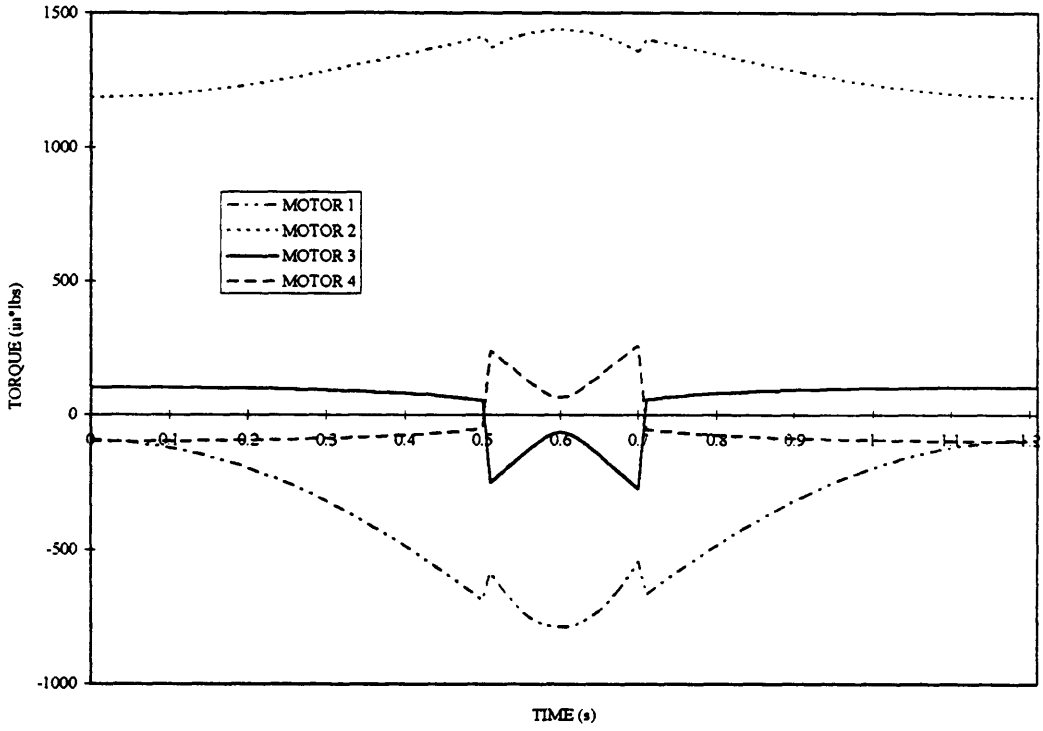

Fig. 4.17: The torques trajectories to apply a force

The optimal trajectory shown in Figure 4.16 moves the centroid of the robot to just before the arm reaches a singular configuration. This would imply that the optimization find a minimum when a force can be borne near a singular configuration. Since the torque required at a singular configuration would be zero for an infinite load.

Using the mechanical advantage ellipsoids presented in Section 2.9, we can examine several instances during the trajectory. Figure 4.18 shows the ellipses superimposed onto the centroid and end-effector for two configurations. In the initial position the arm is not in a favorable configuration to produce a force at the end-effector. We see that in the second configuration, just before the singularity of the arm, the ellipse is elongated in the horizontal direction. This elongation show the large mechanical advantage the arm has in this configuration.

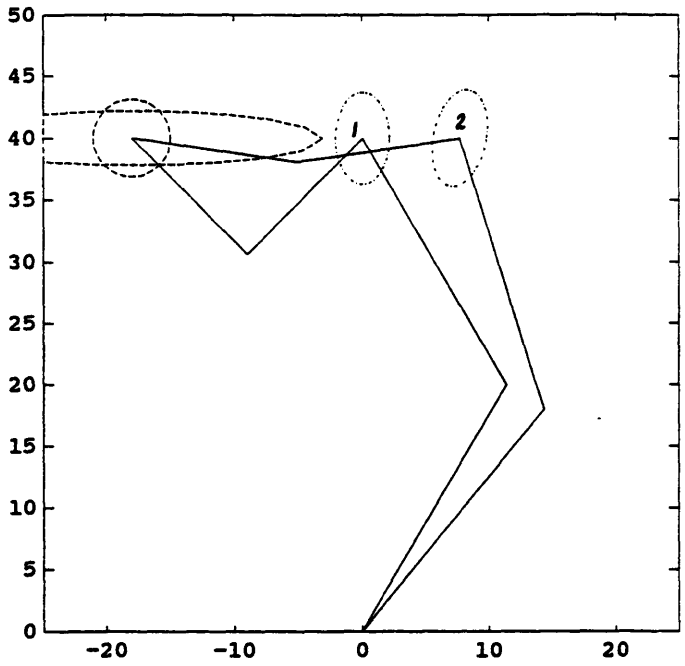

Figure 4.18 Mechanical Advantage superimposed on configurations for dynamic pull

A quasi-static method is used to compare the dynamic method. For the quasi-static comparison method the robot torques are computed for the case of applying an identical force for the same duration as the dynamic method. For this comparison case the robot remained in the initial configuration of the dynamic method for the entire duration. The force at the end-effector are the same for both cases but the forces produced at the base are different. The quasi-static case produces forces at the base that are equal but opposite in direction to the forces produced at the end-effector. The dynamic case produces forces at the base associated with accelerating the body mass. This is analogues to the forces measured for the case of a human producing a force to a stuck door using these two methods which is shown in Figures 3.2 and 3.3.

These two methods can be compared by computing the temperature rise of each motor from the torque trajectories as was done for the lifting example. The results of this computation is shown in Figure 4.19.

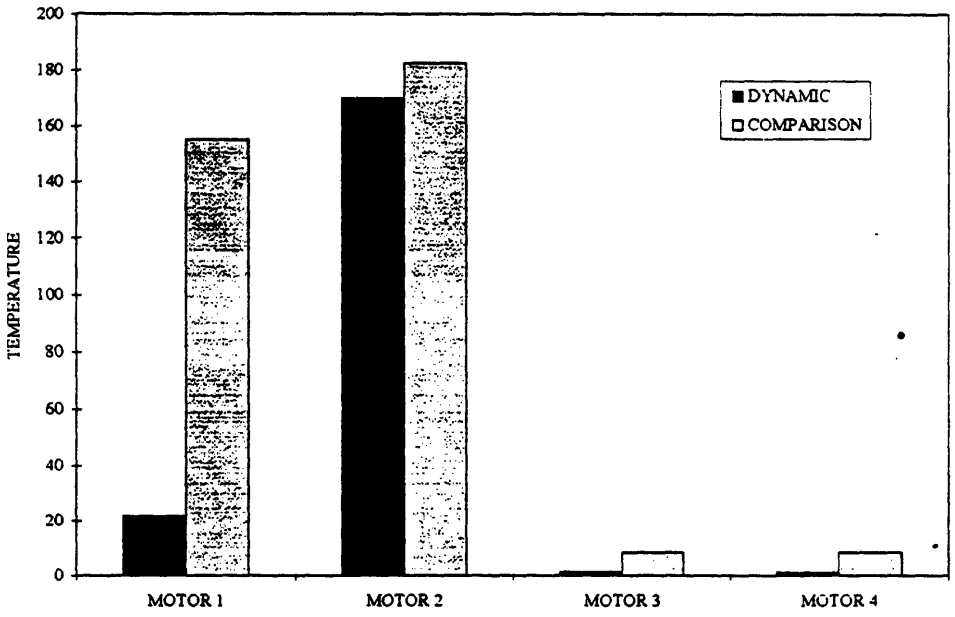

Fig. 4.19. Temperature rise comparison for pull

The temperature rise is less for each motor for this example. Summing the temperatures of all the motor for each method we can compute a value that is proportional to the energy dissipated. The dynamic method for this case was found to use 45% less dissipated energy than the comparison trajectory for this example. This large difference can be attributed to the inefficient operation of the actuators operating in stall torque mode for the quasi-static case.

4.4 Model Re-design and Re-optimization

From the results in the previous section we can redesign our robot model for better performance. Using this new model we can repeat the trajectory optimization process to find a new optimal trajectory.

In Figure 4.15 and 4.19 the temperature rise of motor 1 and 2 can be seen to be much hotter than motor 3 and 4 for each of the tasks. Using this information we redesign our robot model by increasing the size (thermal capacity) of motor 1 and 2 so that the temperature rise of these motors are comparable with the temperature rise of motors 3 and 4. If motor 1 and 2 of our robot model are doubled in size than the temperatures created for the exemplary tasks would be of the same order.

Using this new robot design the trajectory for the lifting task was re-optimized. The results of this optimization can be seen in Figure 4.20. The trajectory found in this case

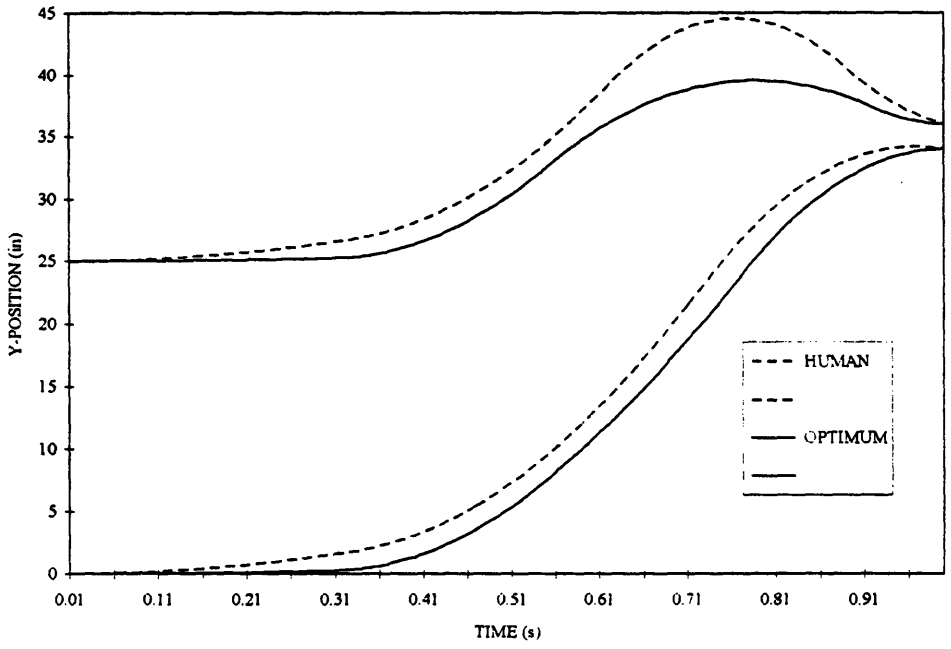

Fig. 4.20 Lift trajectories optimized with redesigned model

more closely resembles the human trajectory than the optimum shown in Figure 4.10 found using the old model. Again the torque trajectories can be computed from the optimal and comparison trajectories. Using the torque trajectories the temperature rise for each motor can be computed. The temperature rise was computed for the case of the new optimum is compared to the same comparison trajectory that was used in the previous lifting task. Figure 4.21 shows the results of this simulation.

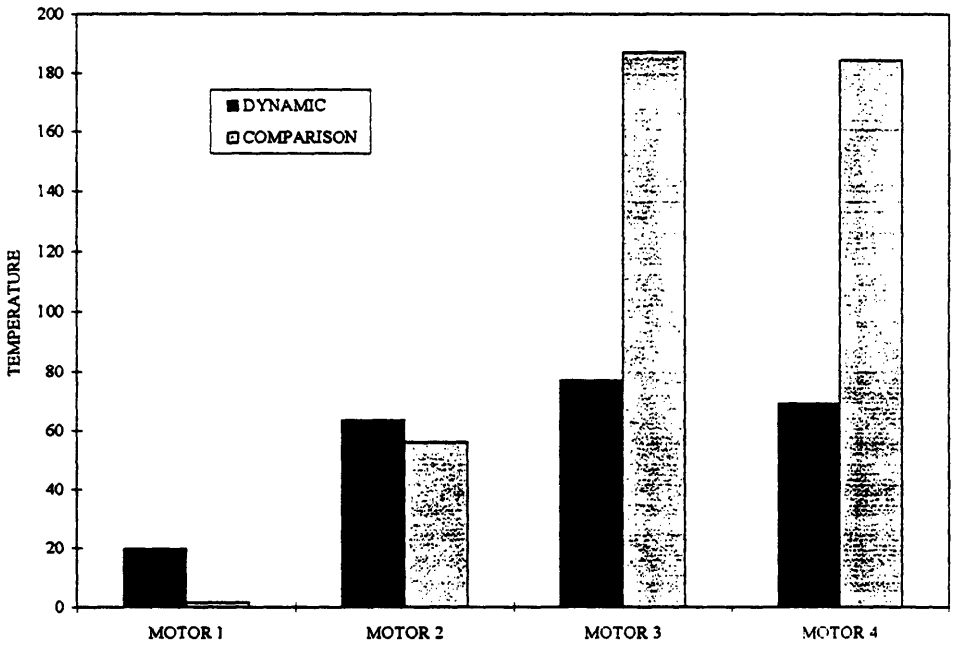

Fig. 4.21. Temperature rise for redesigned robot performing lift

Although the temperature rise of motor 1 and 2 are greater for the this new dynamic case the benefit of this lift is apparent from the large difference of motor 3 and 4 which are much cooler for the dynamic case. Computing the energy dissipated for the lifting task shows that the dynamic method optimized for the new model requires 46% less dissipated energy than the comparison trajectory. The result found for this task using the previous robot model was found to require 7% less dissipated energy.

Chapter 5
The Design of a Prototype Robot

In this chapter the design and construction of a prototype robot will be described. This robot will be used to test the concepts of producing dynamic forces and lifting using a dynamic technique. We will begin the design by addressing the theoretic issues for the ideal design features of a planar robot designed specifically to perform dynamic tasks. The construction issues will be addressed which include the structure, materials, transmission, bearings, and actuator. The final design will be presented and the results of the experiments performed will be presented in Chapter 6.

5.1 Theoretical Design Issues

As we found in Chapter 2 many practical dynamic tasks can be accomplished if a robot has the ability to move its end effector independently from the center of mass. This functionality can be achieved by designing the robot so that it meets the redundancy criterion. To be able to move the end effector separately from the center of mass, for each dimension of operation, there must be robot mass that can be controlled to move in the same direction or the opposite direction as the end effector. To achieve this criterion the robot should be designed such that for each dimension of operation of the end effector there are at least two degrees of freedom.

In this thesis we will examine the case of two dimension motion. To meet the redundancy criterion a four degree of freedom robot is needed. A serial chain of four links is selected for the design of our robot (see Figure 5.1). In Chapter 2 we found that by placing the majority of the robots mass in the middle of the serial chain of links that make

up the redundant robot the robot's mass can be utilized most effectively. For our design one way of placing most of the mass in this location is to place all of the actuators at this location (one of the heaviest components of the robots is its actuators). By designing the links to be as light as possible the actuator torques can be utilized for moving the center of mass most effectively.

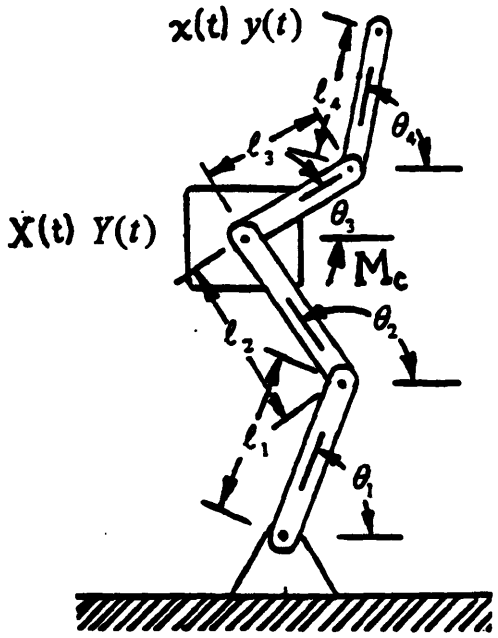

Figure 5.1: Planar dynamic robot model

Links 3 and 4 should be designed with a shorter length (15%-20%) than links 1 and 2. This length difference allows the centroid of the robot to be positioned in a wide variety of positions relative to the endeffector. This length difference also allows links 3 and 4 to have singular points in a large range of the robots workspace. These singular points facilitate mechanical advantages that can vary widely.

5.2 Structural Design Issues

The structural design issues are addressed in this section. These are issues that have to do with how the structure of the robot will be designed to accomplish the desired motion and load bearing.

The prototype robot will be designed to demonstrate the production of dynamic forces. Since these forces are quite large, load bearing considerations are very important. Two ways of designing a revolute joint between two links are 1) stacking the two links on the revolute joint so that the two links are side by side and 2) the two links are designed to be in line and the two links intersect at the joint. The first method allow larger mobility of the joint (360 degrees are possible), but the load handling capabilities are not as large compared to the second case. The second case does allow a larger load handling capability but the mobility is limited (approximately 250 degrees). The second method was chosen for the design of our robot for the larger load handling capabilities. To make up for the limited mobility of this design off-centered pivot locations where chosen. These off-centered pivots allow the mobility to increase for small angles between two links but decrease mobility for hyper-extended configurations. The off-center pivots provide the arm with the most mobility in terms of the workspace from being fully extended to fully contracted (links at sharp angles to each other).

The motor assembly was designed so that it could be manually pivoted into three configurations. This pivoting provides a greater range of workspace needed for testing a variety of dynamic tasks. Figure 5.2 shows the design for the prototype robot.

The transmission system selected for our robot is a gear head motor with timing belts to transmit the torque to each joint. Planetary gear heads were chosen for there ability to sustain a large torque for a small package. In addition to the mechanical advantage from the gear head, an additional mechanical advantage was received from the pulleys and timing belts. This gear reduction from the belts, besides providing additional mechanical advantage, helps to reduce the effect of back-lash from the motor gear head.

Although the belts are relatively stiff they provide some compliance and damping into the system. These properties will help to alleviate the structure and bearings from having to bear very large forces caused from high impacts.

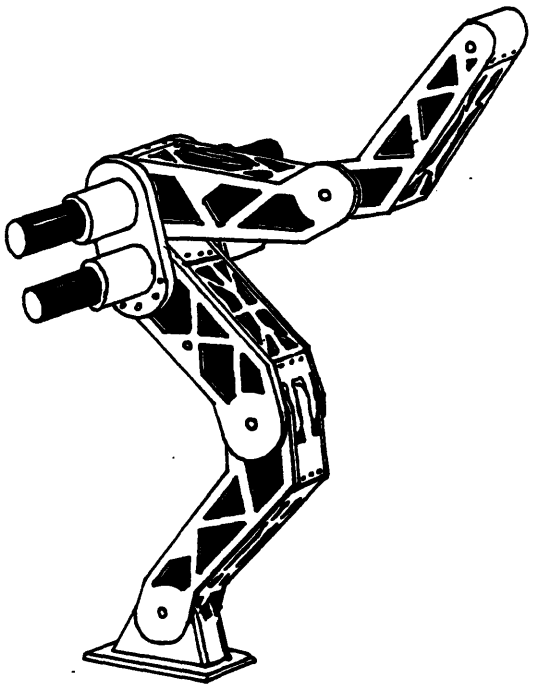

Figure 5.2: The design of a planar dynamic robot

5.3 Construction Design Issues

The robot was constructed from 6061 T6 aluminum plate and milled out with a structured pattern to reduce the weight of the links. These plates have been attached to form a box beam for each link. The revolute joints where designed with the outside plates of the box beam connected together by an axil. Large diameter axils (one inch) were used to give added structural support for these two plates in torsion. The connecting link was designed to ride on these axils with high load rated deep groove ball bearings captured by the two plates of the connecting link.

The actuators are 4 DC permanent 'rare earth' magnet motors and are equipped with air cooling. Low pressure air is pumped in at an inlet on each motor near the brushes and commutators. The air flows past the motor's armature and exits just below the gear head. The motor's armature has been designed with low inertia to allow high angular accelerations. The motors were fitted with HP optical encoders with 256 lines per revolution. These encoders where used to control the position of the robot. Each motor has a planetary gear head with a gear ratio of 55.4:1. These motors are distributed to each of the joint through a series of Kevlar reinforced timing belts. Idler cams were used to tension the belts. The arrangement of these belts is shown in Figure 5.3. Motor 1 drives the ankle joint by two belts with an idler pulley located in-between at the knee joint. Motor 2 drives the knee joint by a single belt. The shoulder joint is driven directly by motor 3 and the elbow joint is driven by motor 4 through a belt.

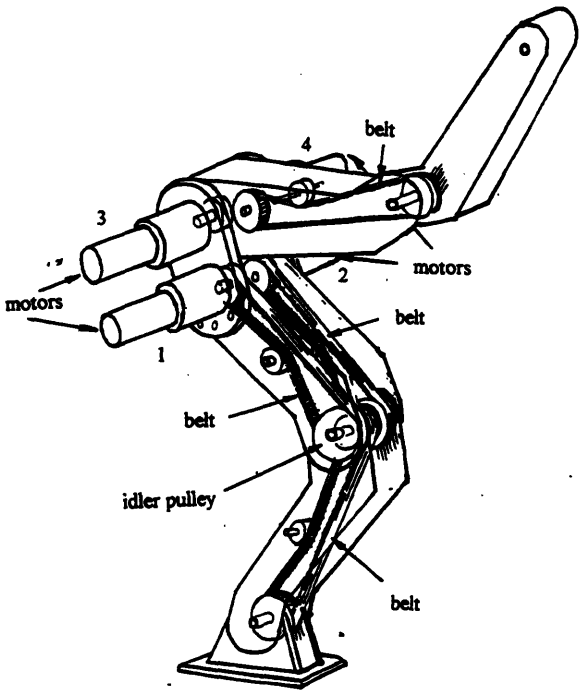

Figure 5.3: Internal structure of the dynamic robot

5.4 Control System Hardware

Aerotech DS16030 amplifiers were used to power the four motors. The encoder signals were read by a Technology 80 5312 encoder board installed in a 486 50MHz computer. The robot was controlled using PD control done discretely with a C program on the computer. As a safety precaution the output power of each amplifier was fed through a relay. Several emergency switches where setup so that if any one of the switched was not closed the relays would disconnect the motors from the amplifiers. In addition to being disconnected from the amplifiers the relays would short out the motors using the back emf as a dynamic break. Figure 5.4 shows a photograph of the completed prototype and control system.

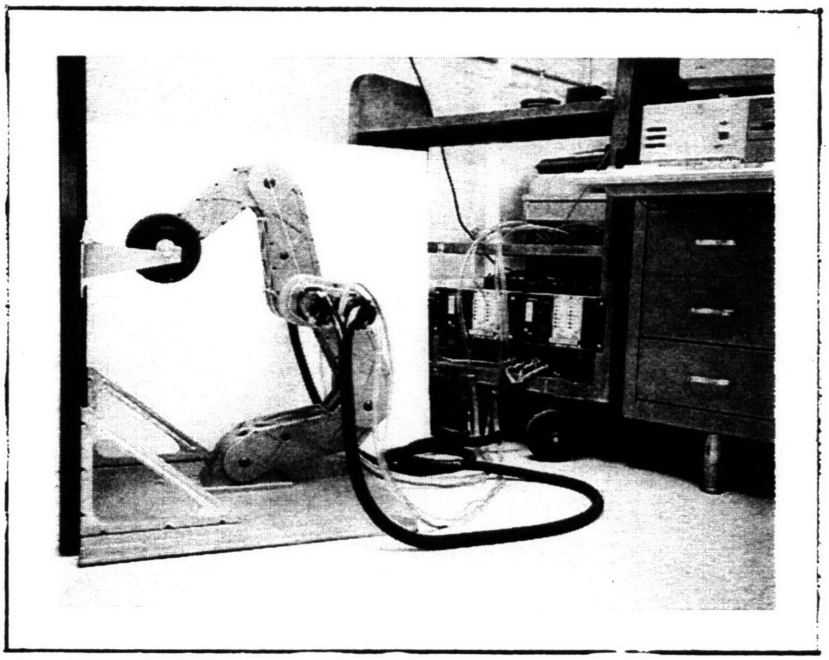

Figure 5.4: Photograph of prototype robot and control system

Chapter 6
Experimental Verification

In this chapter, the prototype robot will be experimentally tested. Two dynamic task will be addressed, applying forces and lifting using a dynamic technique. These dynamic tasks were compared to comparison tasks that do not use a coordinated motion to accomplish the same goal. Thermistors were placed on the motors and the temperature before and after each task was measured. The temperature rise was compared for the dynamic technique and the comparison technique. The results of these measurements are presented and discussed in the following sections.

6.1 Experimental Setup

The prototype robot described in Chapter 5 was mounted to a base. The prototype was connected to the power amplifiers and the amplifiers where connected to an D/A board located in the computer. The encoders of each motor were also connected to the computer through the counting board. The robot was controlled using a C program that takes a preprogrammed trajectory and controls the robot to move through the trajectory using PD control. Thermistors were placed inside each of the motors at the outlet of the air cooling holes. These thermistors were connected to amplifier boards so that the temperature that they measured could be recorded.

6.2 Procedure

Two lifting task was tested. The task was to lift a heavy object using a dynamic method. Trajectories for each of these tasks were developed using the method described in Chapter 4. For this dynamic tasks a comparison trajectory was developed. The comparison trajectory for the lifting case is similar to the comparison trajectory discussed in Chapter 4.

The trajectory developed was for a weight of 20 lbs. The experiments began with a small weight (to be cautious not to damage the robot) and increased to the programmed weight and beyond. For each weight, twenty runs were measured, ten for the dynamic method and ten for the comparison trajectory. For each run the temperature rise of each motor was recorded. These temperatures were average for the ten runs for each method.

6.3 Results

The temperature rise measured of each motor for the task of lifting 7 lbs. is shown in Figure 6.1 for the dynamic case and the comparison case. Notice the temperature rise for motor 3 and 4 are greater for the comparison case. Figure 6.2 shows the temperature rise of each motor for the task of lifting 14 lbs.

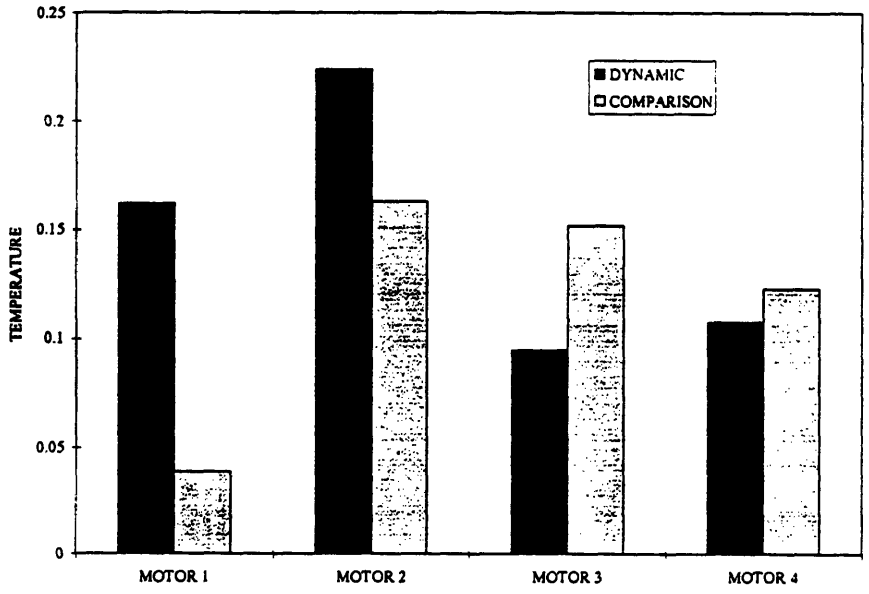

Fig. 6.1: Temperature rise for dynamic vs. comparison lift of 7 lbs.

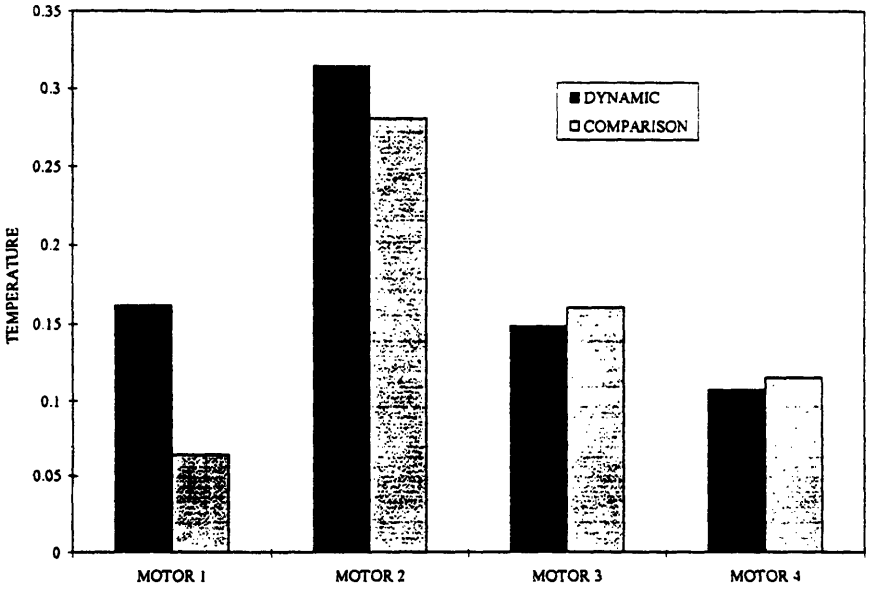

Fig. 6.2: Temperature rise for dynamic vs. comparison lift of 14 lbs.

In this case the motors 3 and 4 are again less for the dynamic case but not as significantly as for the 7 lbs case. Note also that motor 2 for both cases is the hottest motor and the dynamic method is hotter. Figure 6.3 shows the temperature rise of each motor for the task of lifting 19 lbs.

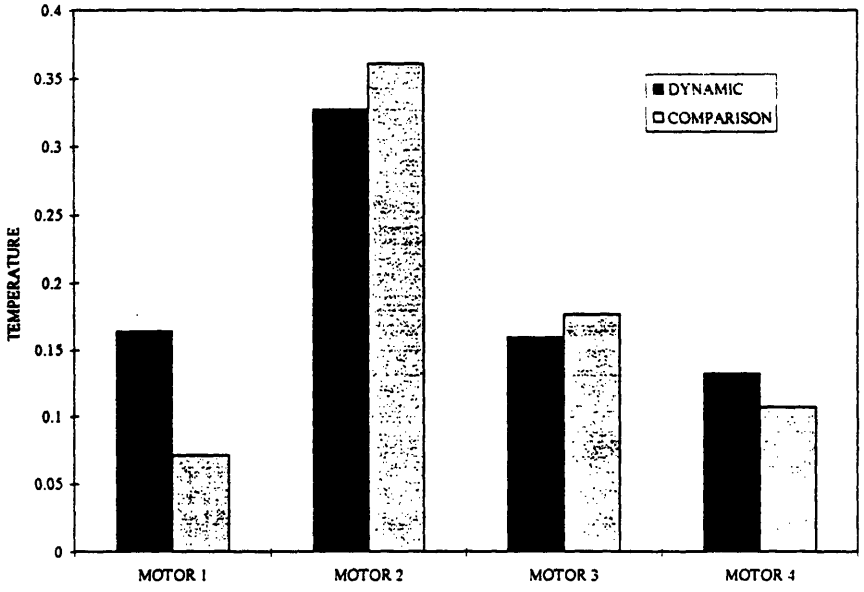

Fig. 6.3: Temperature rise for dynamic vs. comparison lift of 19 lbs.

For the 19 lbs. case motor 2 is again the hottest but now the comparison method is the hottest. Motor 3 is also hotter for the comparison method in this case. Figure 6.4 shows the temperature rise of each motor for the task of lifting 25 lbs.

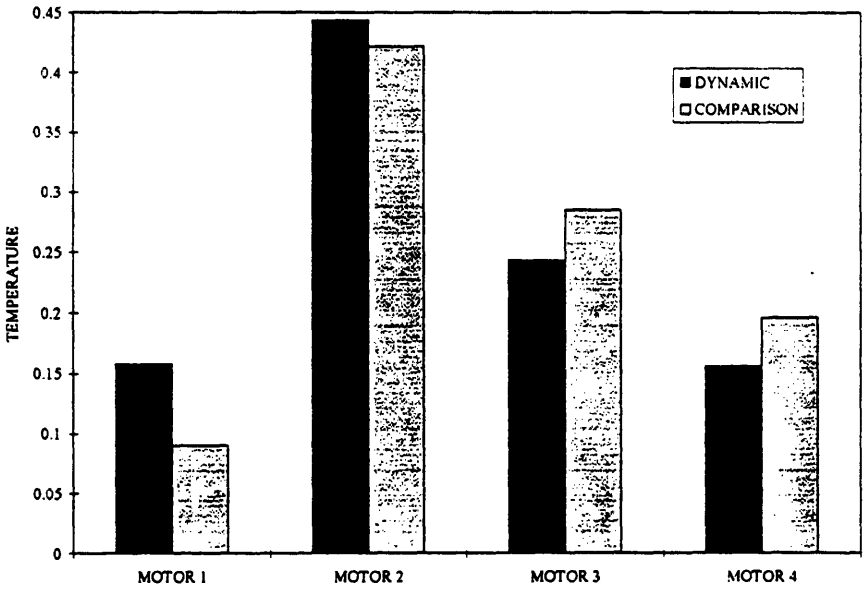

Fig. 6.4: Temperature rise for dynamic vs. comparison lift of 25 lbs.

In the case of the robot lifting 25 lbs. motor 2 is again the hottest. Motor 2 for the dynamic method is hotter than the comparison method similar to the cases of the first two weights. Again motor 3 and 4 are hotter for the comparison method.

6.4 Discussion

The trajectory for this experiment was optimized for the weight of 20 lbs. The optimization program tries to find a trajectory that minimizes the hottest motor. In this example the hottest motor is always motor 2. The only case where the rise in temperature of motor 2 is less for the dynamic method is for the case of lifting 19 lbs. This uniqueness can be explained by noticing that the trajectory was optimized for 20 lbs. It is understandable that the dynamic motion of the robot is moving according to the weight specified in the optimization. If this weight is not the one specified there will be additional

dynamic forces that exist to balance the motion. These additional forces cause the robot to use more energy than a true optimized dynamic system would require.

This aspect of the dynamic method show the need to know the weight of the object being lifted. If the weight of the object being lifted is known then the robot could compute an optimal trajectory to use the dynamic method.

From the experiments the temperature of motor 2 was found to be 9% less hot as the comparison trajectory method. The simulation of a similar robot model predicted a 7% difference. These percentages show relatively good agreement between the experimental and simulated results. The reason for the small discrepancy between the experimental and simulated results may be due to an inaccurate robot model or inaccurate measurements.

With an improved robot model the simulation predicted that a robot could lift using 46% less dissipated energy applying a dynamic method than a comparison method. By modifying our robot prototype in terms of this new model we would expect a similar experimental result.

Chapter 7
Conclusion

A dynamic robot was designed with and applied to the task of producing forces and lifting mass. In Chapter 2, we identified the redundancy criterion which describes the kinematic robot structure that allows independent control of the robots centroid and end effector. A method for finding actuator torques from centroid and endeffector trajectories was found. The form of our dynamic robot was found to be four serial planar links with most of the mass located in the middle (after two links).

In Chapter 3, human dynamic lifts were analyzed in order to find schemes and constraints to design trajectories for the robot.. These measurements were used to find plausible class of tractable trajectories to apply to robotic motion. Humans were measured performing two exemplary dynamic tasks. The forces and motions were measured of humans performing the tasks of trying to open a stuck door and lifting objects.

In Chapter 4, a method is presented for computing trajectories for our robot design for the tasks of creating forces and lifting objects. A performance index based on the internal temperature of the robots actuators was found. Trajectories were parameterized based on the human motion. By starting with the human trajectories as initial estimates optimal trajectories for our robot were found using the performance index. We found that the optimal trajectory needed larger peak torque but smaller average torque than the constant acceleration trajectories. Although the peak torque required is higher this scheme is much more favorable for robots because electric motors are much better suited to produce short high torques than extended moderate torques. The dissipated energy for the tasks of lifting objects and applying forces was computed. The initial robot design with all

actuators weighted equally showed that the dynamic method required 7% less dissipated energy for the lifting task and 46% less energy dissipated for the task of applying forces using the dynamic method compared to a traditional method. After weighting the base motors by two times the simulation showed a 45% less dissipated energy need to complete the lifting task.

In Chapter 5, the design and construction of a prototype robot was described. This robot was used to test the concepts of producing dynamic forces and lifting using a dynamic technique. The theoretic issues for the ideal design features of a planar robot designed specifically to perform dynamic tasks were presented. The construction issues were addressed which include the structure, materials, transmission, bearings, and actuator of our prototype robot.

In Chapter 6, the prototype was tested for the dynamic tasks of applying forces and lifting dynamically. Thermistors were placed on the motors and the temperature was measured after each task. The temperature was compared for a dynamic technique and a comparison technique. The prototype robot was found to agree closely with the simulation.

In this thesis a new method in robotics was explored for performing dynamic tasks. The theoretical basis was presented. The critical design features to accomplish dynamic tasks were developed. Human dynamic motion was examined to inspire new techniques for robotics. Trajectory synthesis methods were developed for lifting objects and producing forces to the environment. Simulation of dynamic lifting and door opening task were performed. The simulation showed that the dynamic method uses 46% less dissipated energy than a comparison method. A proof-of-concept dynamic robot was designed, built and tested. The prototype robot was found to agree closely with simulation.

REFERENCES

Arai, T., Osumi, H., "Construction System of Heavy Parts by the Coordinated Control between a Crane and a Robot," Ninth Int. Symp. on Automation and Robotics in Construction, Tokyo, 1992.

Amirouche, F.M.L.,"Dynamic Analysis of Lifting-Redundancy Modeling and Motion Control Parameters Identification," Presented at the 1993 ASME Winter Annual Meeting, New Orleans, LA, 1993.

Asada, H. "Dynamic Analysis and Design of Robot Manipulators Using Inertia Ellipsoids", IEEE Computer Society 1st International Conference on Robotics, Atlanta, Georgia, March 13-15, 1984, pp. 94-102.

Asada, H., and Asari, Y., "The Direct Teaching of Tool Manipulation Skills Via the Impedance Identification of Human Motions," IEEE International Conference on Robotics and Automation, 1988, pp 1269-1274,

Asada, H. and Granito, J.A.C., "Kinematic and Static Characterization of Wrist Joints and Their Optimal Design," IEEE International Conference on Robotics and Automation, 1985, pp. 244-250.

Asada, H., and Slotine, J.-J., *Robot Analysis and Control*. John Wiley and Sons, 1986

Baillieul, J., "Avoiding Obstacles and Resolving Kinematic Redundancy," Proc. IEEE Int. Conf. Robotics and Automation, 1986.

Brady, J.M., Hollerbach, J.M., Johnson, T.L., Lozano-Pérez, T., and Mason, M.T., eds., *Robot Motion: Planning and Control*, MIT Press, Cambridge, Massachusetts, 1982

Brown, K., The Design and Analysis of Zero Reaction Force Robots, M.S. Thesis, MIT Department of Mechanical Engineering, June, 1990.

Brown, K., and Asada H., "Design and Control of a Dynamic Robot Inspired by Dynamic Human Motion," Presented at the 1993 ASME Winter Annual Meeting, New Orleans, LA, 1993.

Brown, K., and Asada H., "Learning Dynamic Task Strategies from Humans for the Design and Control of Heavy-Duty Robots," To be Presented at the 1994 ASME Winter Annual Meeting, Chicago, IL, 1994.

Carlsöö, S., How Man Moves. William Heinemann Ltd., 1972.

Frievalds, A., Chaffin, D. B., Garg, A., and Lee, K.S., "A Dynamic Biomechanical Evaluation of Lifting Maximum Acceptable Load," Journal of Biomechanics, Vol. 17, 1984, pp.251-262.

Fujii, N., "A General Simulation System of Two-Dimensional Multi-Link Model of Human Body", International Society of Biomechanics, XII Congress, 1989.

Fukuda, T., Fujisawa, Y., Kosuge, K., Fumihito, A., Muro, E., Hoshino, H., Miyazaki, T., Ohtsubo, K., Uehara, K., "Gravity Center Control for Manipulator/Vehicle System for Man-Robot Cooperation," Ninth Int. Symp. on Automation and Robotics in Construction, Tokyo, 1992.

Funato, K. and Fukunaga, T., "Mechanical Power Developed During Pull Movement in Weightlifting," International Society of Biomechanics XII Congress, 1989.

Gagnon, M. and Smyth, G., "Muscular Mechanical Energy Expenditure as a Process for Detecting Potential Risks in Manual Materials Handling," Journal of Biomechanics, vol. 24, no.3/4 pp. 191-203, 1991.

Hollerbach, J. M., "A Recursive Formulation of Lagrangian Manipulator Dynamics," IEEE Trans. Systems, Man, Cybernetics, Vol. 10, No. 11, 1980.

Hu, Y. R. and Goldberg, A. A., "Dynamic Control of Multiple Coordinated Redundant Robots", IEEE Transactions on Systems, Man, and Cybernetics, Vol. 22, No 3, May/June 1992.

Khatib, O., "Dynamic Control of Manipulators in Operational Space," Sixth IFTOMM Congress on Theory of Machines and Mechanisms, New-Delhi, 1983.

Kitamura, S, Kuramoatou, Y. and Nakai, Y., "Application of the Neural Network for the Trajectory Planning of a Biped Locomotive Robot", International Neural Network Society, 1988 First Annual Meeting, Boston, MA, September, 1988.

Kromodihardjo, S. And Mital, A., "Biomechanical Analysis of Manual Lifting Tasks", Journal of Biomechanical Engineering, Vol. 109, May 1987, pp. 132-138.

Lee, T. T. and Liao, J., "Trajectory Planning and Control of a 3-Link Biped Robot", Proceedings-1988 IEEE International Conference on Robotics and Automation, Philadelphia, April 1988.

Lee, T. T. and Shih, C. L., "An Approach for Robotic Motion Planning With Control Torques and Obstacle Constraints", IEEE International Conference on Robotics and Automation 1990.

Lee, W.A. "Learning to Control Body Center of Mass During Arm Pulls Made While Standing" Posture and Balance: Control Mechanisms, M.H. Woollacott and F. Horak (eds.), University of Oregon Press, Eugene, Oregon, 1992, pp. 364-367.

Luh, J. Y. S. and Walker, M. H., "Minimum-Time Along the Path for a Mechanical Arm," Proceedings IEEE Conference Decision and Control, New Orleans, Louisiana, 1977, pp. 755-759.

Luh, J. Y. S., Walker, M. H. and Paul, R. P. C., " Resolved Acceleration Control of Mechanical Manipulators," IEEE Trans. Automatic Control, Vol. 25, No. 3, 1980.

Maciejewski, A.A. and Klein, C.A., "Obstacle avoidance for kinematically redundant manipulators in dynamically vary environments environments," The International Journal of Robotics Research, vol. 4, no.3, pp.109-117, 1985.

Madhani, A. and Dubowsky, S., "Motion Planning of Multi-Limb Robotic Systems Subject to Force and Friction Constraints," IEEE International Conference on Robotics and Automation, Nice, France, 1992.

Matsugaki, K., "Prospects for Applying Automation/Robotization in Concrete Dam Construction," Ninth Int. Symp. on Automation and Robotics in Construction, Tokyo, 1992.

Mayorga, R.V. and Wong, A.K.C., "A Singularities Prevention Approach for Redundant Robot Manipulators," IEEE International Conference on Robotics and Automation, Cincinnati, Ohio, 1990, pp. 812-817.

Michaels, C.F., Lee, W.A., and Pai, Y.C., "The Organization of Multisegmental Pulls made by Standing Humans: I. Near-Maximal Pulls," Journal of Motor Behavior, In press.

Miyatake, Y., Fujimori, T., Ueno, T., "Automation and Robotics in Construction Industry," Shimizu Corporation, Tokyo, 1993.

Nakamura, Y., and Hanafusa, H., "Task Priority Based Redundancy Control of Robot Manipulators," Int. Symp. of Robotics Research, Kyoto 1984.

Nakamura, Y., and Hanafusa, H., "Inverse Kinematic Solutions with Singularity Robustness for Robot Manipulator Control," ASME Jounal of Dynamics Systems, Measurement and Control, Vol. 108, No. 3, 1986, pp. 163-171.

Nakanshi, T., and Hirabayashi, M., "Automatic Control System for the Shield Tunneling Machine," Ninth Int. Symp. on Automation and Robotics in Construction, Tokyo, 1992.

Pandy, M.G., Anderson, F.C. and Hull, D.G.,"A Parameter Optimization Approach for the Optimal Control of Large-Scale Musculoskeletal Systems," Journal of Biomechanical Engineering, Vol. 114, 1992, pp. 450-460.

Papadopoulos , E. and Dubowsky, S., "On the Nature of Control Algorithms for Space Manipulators", IEEE International Conference on Robotics and Automation, 1990.

Pearson, J. R., McGinley, D. R. And Butzel, L. M., " Dynamic Analysis of The Upper Extremity for planar motions," Human Factors, Vol. 5, 1963, pp. 59-70.

Raibert, M. H., "Legged Robots that Balance," M.I.T. Press, 1986.

Sahar, G. and Hollerbach, J.M., "Planning of Minimum-Time Trajectories for Robot Arms," IEEE International Conference on Robotics and Automation 1985, pp. 751-758

Singh, S. K., "Motion Planning and Control of Non-Redundant Manipulators at Singularities," IEEE International Conference on Robotics and Automation 1993, pp.487-491.

Vafa, Z. and Dubowsky, " On the Dynamics of Manipulators in Space Using the Virtual Manipulator Approach," IEEE International Conference on Robotics and Automation, 1987, pp 579-585.

Vukobratovic, M., "Dynamics of Active Articulated Mechanisms and Synthesis of Artificial Motion," Mechanism and Machine Theory, 13, 1978.

Waldron, K. J., Wang, S.-L., and Bolin, S. J., "A Study of the Jacobian Matrix of Serial Manipulators," ASME J. Mech. Trans. & Auto. in Design, Vol. 107, No. 2, 1985.

Wings, R.D., "Robots in Construction--a state of the art review," Proc. Instn Civ. Engrs, Part 1, 1989, 86, Oct., 937-952.

Zvi, S. and Dubowsky, S., "Global Time Optimal Motions of Robotic Manipulators in the Presence of Obstacles," IEEE International Conference on Robotics and Automation 1988 pp.370-375.